# 4E Analysis and Optimization of a Novel Hybrid Biomass-Solar System: Focusing on Peak Load Management and Environmental Emissions

Korpeh, Mobin ; Asadbagi, Poorya ; Lotfollahi, Amirhosein ; Ghaemi, Sina; Anvari-Moghaddam, Amjad

*Published in:*
Process Safety and Environmental Protection

*DOI (link to publication from Publisher):*
10.1016/j.psep.2023.11.035



*Publication date:*
2024

*Document Version*
Publisher's PDF, also known as Version of record

Process Safety and Environmental Protection 181 (2024) 452–468

Contents lists available at ScienceDirect

Process Safety and Environmental Protection

journal homepage: www.journals.elsevier.com/process-safety-and-environmental-protection

# 4E analysis and optimization of a novel hybrid biomass-solar system: Focusing on peak load management and environmental emissions

Mobin Korpeh [a], Poorya Asadbagi [a], Amirhosein Lotfollahi [a], Sina Ghaemi [b], Amjad Anvari-Moghaddam [b,*]

[a] School of Mechanical Engineering, Iran University of Science and Technology, Tehran, Iran
[b] Department of Energy (AAU Energy), Aalborg University, 9210 Aalborg, Denmark

ARTICLE INFO

*Keywords:*
Renewable energy
Hybrid biomass-solar system
PEM electrolyzer
Multi-effect desalination
Multi-objective optimization

ABSTRACT

Renewable energies are available as clean sources to replace fossil fuels. Providing continuous power without compromising the environment through hybridizing solar and biomass source is one of the promising solutions. This paper seeks to address thermodynamic, economic, and environmental analysis of a multi-generation system with the aim of supplying heating, cooling, electricity, fresh-water, and hydrogen. To do this, the considered system is divided into on-peak, mid-peak, and off-peak periods and modeled based on the consumption pattern at different hours of the day and night. Due to the availability of renewable energy during peak consumption periods, biomass, solar, and hybrid biomass-solar energies are used as energy sources. This leads to a reduction in biomass consumption and carbon dioxide emissions through storing approximately 10 tons of biomass during the day. A sensitivity analysis of the factors affecting the system's function indicated that a growth in solar radiation from 600 to 1000 W/m$^2$, results in a 35% improvement in exergy efficiency, a 2.7% raise in the total cost rate, and a 32.4% drop in $CO_2$ emissions of the system. Moreover, by changing the biomass flow rate from 0.5 to 1.5 kg/s, the exergy efficiency and total cost rate improved by 9.28%, 1.3%, respectively, and the $CO_2$ emissions rate increased from 0.41 to 1.14 tons/MWh. In addition, focusing on addressing economic and environmental concerns, the optimization of the proposed hybrid system is performed in two categories of objective functions. In the second category optimization, exergy efficiency, fresh water production, total cost rate and $CO_2$ emissions are determined as 31.75%, 74.75 kg/s, 324.60 $/h and 3.55 tons/MWh, respectively.

## 1. Introduction

More energy demand and environmental problems have led to more use of renewable sources. amongst them, solar energy is the cleanest and most plentiful source of energy. Solar source depends on both power of the sun and the number of hours it can be received. Another critical renewable resource is biomass, which has played an important role in human life since the beginning of human existence. The most common biomass sources are agricultural products, marine plants, and forest materials. The Global Energy Assessment reports that the amount of energy supplied by biomass is about 9.5% (Devi et al., 2003).

Each renewable energy source has unique characteristics that make it usable in certain conditions. Solar energy, despite its abundance, is intermittently unavailable at night or on cloudy days due to its dependence on environmental conditions. On the other hand, biomass energy is continuously available regardless of weather conditions, but its combustion releases carbon dioxide into the atmosphere. Consequently, combining energy sources in energy systems has become increasingly important to improve the efficiency of thermodynamic cycles (Bet Sarkis and Zare, 2018a).

The synergy between biomass and solar energy presents a viable combination that can be effectively implemented in multi-purpose systems, offering a consistent and dependable energy source. In recent years, extensive research has been conducted on the integration of biomass and solar energy in multi-generation systems, further establishing its feasibility and potential. Anvari et al. (2018) used biomass combustion energy with a solar turbine and steam Rankine cycle (SRC) to generate power in their hybrid system. The use of hybrid biomass-solar compared to the use of biomass energy source alone causes a 30% increase in electricity production and a 22% decrease in $CO_2$ emissions. To achieve continuous energy, Suresh et al. (2019) combined biomass and solar energy and designed a hybrid biomass-solar power plant with a steam Rankine cycle that utilizes both electrical and

* Corresponding author.
*E-mail address:* aam@energy.aau.dk (A. Anvari-Moghaddam).

https://doi.org/10.1016/j.psep.2023.11.035
Received 8 August 2023; Received in revised form 9 November 2023; Accepted 18 November 2023
Available online 23 November 2023

**Nomenclature**

| | |
|---|---|
| $A_{hel}$ | Overall area of heliostat field ($m^2$) |
| $A_{rec}$ | Receiver aperture area ($m^2$) |
| $Cp_x$ | Specific heat capacity of x ($J/mol.℃$) |
| $CR$ | MED compression ratio |
| $D$ | Membrane thickness of PEME ($\mu m$) |
| $E$ | Input energy rate ($kW$) |
| $\dot{E}x$ | Exergy rate ($kW$) |
| $\dot{E}x_{d,x}$ | Exergy destruction in component x ($kW$) |
| $F$ | Faraday constant ($C/mol$) |
| $GTIT$ | High pressure gas turbine inlet temperature ($K$) |
| $h$ | Specific enthalpy ($kJ/kg$) |
| $H$ | Height of the solar tower ($m$) |
| $HHV$ | Higher heating value ($kJ/mol$) |
| $i$ | interest rate (%) |
| $J$ | PEME current density ($A/cm^2$) |
| $J_i^{ref}$ | Pre-exponential factor ($A/m^2$) |
| $J_0$ | PEME exchange current density electrolysis ($A/m^2$) |
| $LHV$ | Lower heating value ($kJ/kg$) |
| $\dot{m}$ | Mass flow rate ($kg/s$) |
| $N_{hel}$ | Number of heliostats |
| $P$ | Pressure ($kpa$) |
| $P_x$ | Partial pressure of x ($kpa$) |
| $\dot{Q}$ | Heat transfer rate ($kW$) |
| $R$ | Universal gas constant ($kJ/kmol.K$) |
| $R_{PEM}$ | Ohmic resistance of PEME (Ω) |
| $s$ | Specific entropy ($kJ/kg.K$) |
| $S$ | Motive steam flow rate ($kg/s$) |
| $T$ | Temperature (℃) |
| $T_0$ | Ambient temperature (℃) |
| $T_{PEME}$ | Operating temperature of PEME (℃) |
| $V$ | Overpotential (V) |
| $V_0$ | Reversible potential (V) |
| $V_{act}$ | Activation potential (V) |
| $V_{ohmic}$ | Ohmic potential (V) |
| $\dot{W}$ | Power consumption or generation ($kW$) |
| $X_{fs}$ | Feed seawater salinity |
| $Z$ | Investment cost ($) |
| $\dot{Z}$ | Cost rate ($/h) |

*Abbreviations*

| | |
|---|---|
| *DNI* | Direct normal irradiance ($W/m^2$) |
| *GA* | Genetic algorithm |
| *MED* | Multi-effect desalination |
| *ORC* | Organic Rankine cycle |
| *PEME* | Proton exchange membrane electrolyzer |
| *SRC* | Steam Rankine cycle |

*Subscripts*

| | |
|---|---|
| *a* | Anode |
| *AC* | Air compressor |
| *act* | Activation |
| *c* | Cathode |
| *CC* | Combustion Chamber |
| *ch* | Chemical |
| *Comp* | Compressor |
| *en* | Energy |
| *ex* | Exergy |
| *Eva* | Evaporator |
| *GT* | Gas turbine |
| *GTHP* | High pressure gas turbine |
| *GTHP* | Low pressure gas turbine |
| *HEX* | Heat exchanger |
| *HRSG* | Heat recovery steam generator |
| *kn* | Kinetic |
| *ph* | Physical |
| *pt* | Potential |
| *Q* | Heat |
| *rec* | receiver |
| *W* | Power |

*Greek symbols*

| | |
|---|---|
| $\lambda$ | Water content |
| $\eta_{cos}$ | Cosine effect efficiency |
| $\eta_{s\&b}$ | Shading and blocking efficiency |
| $\eta_{int}$ | Interception efficiency |
| $\eta_{att}$ | Atmospheric attenuation efficiency |
| $\eta_{ref}$ | Reflectivity efficiency |
| $\eta_{field}$ | Solar power tower heliostat field efficiency |
| $\phi$ | Maintenance factor |

thermal storage. Pantaleo et al. (2020) investigated the thermodynamic analysis and techno-economic evaluation of a combined system of a biomass fueled external gas turbine and an organic Rankine cycle (ORC). In this analysis, thermal energy storage (TES) is used to compensate for solar collector fluctuations. Nami et al. (2021) proposed the use of a solar-assisted biomass-based tri-generation system to provide power, heating and cooling. This system provides an efficient and sustainable solution to meet domestic energy needs. Cao et al. (2021a) proposed using solar renewable energy to produce hydrogen. The hydrogen produced by the thermal photovoltaic panels is added to the combustion chamber and then reacts with the gases resulting from biomass fuel and air combustion.

Also, Jie Ling et al. (2022) conducted a study focused on enhancing the role of solar heat, particularly in the upper cycle of a hybrid system. Their work aimed to minimize the limitations and optimize the efficiency of the system by effectively combining and leveraging the benefits of both biomass and solar energy. To provide the energy required for the hydrogen production process along with the electrical energy production, Burulday et al. (2022) designed a solar power plant integrated with a biomass-based hydrogen production system. They reported an exergy efficiency of 55.8% for the hydrogen production process and 39.6% for the power generation systems. Kumar et al. (2022) conducted a case study on addressing the energy needs of energy-deficient rural communities. The study focused on utilizing locally available energy sources such as solar, biomass, and diesel. Notably, the results demonstrated that integrating solar energy into the optimal system model yielded impressive returns. Altayib and Dincer (2022) presented a hybrid system with constant useful outputs by controlling biomass combustion based on solar radiation changes. The results of this design showed that during periods of maximum solar radiation, biomass consumption can be reduced up to three times compared to night. In order to reduce $CO_2$ emissions and biomass consumption in renewable energy systems, Cao et al. (2022a) combined hydrogen produced by solar energy with biomass gasification-SOFC system. Exergy efficiency, $CO_2$ emission in this configuration was reported as 24.85%, 0.257 kg/kWh, respectively. On the other hand, Oner and Dincer (2022) proposed a new integrated system based on solar energy and biomass for the production of electricity, heating, fresh water and ethanol. By reporting energy efficiency of 53.4% and exergy efficiency of 41%, the authors showed that such hybrid systems are thermodynamically and environmentally more valuable and compatible. The study of the environmental performance of such hybrid power

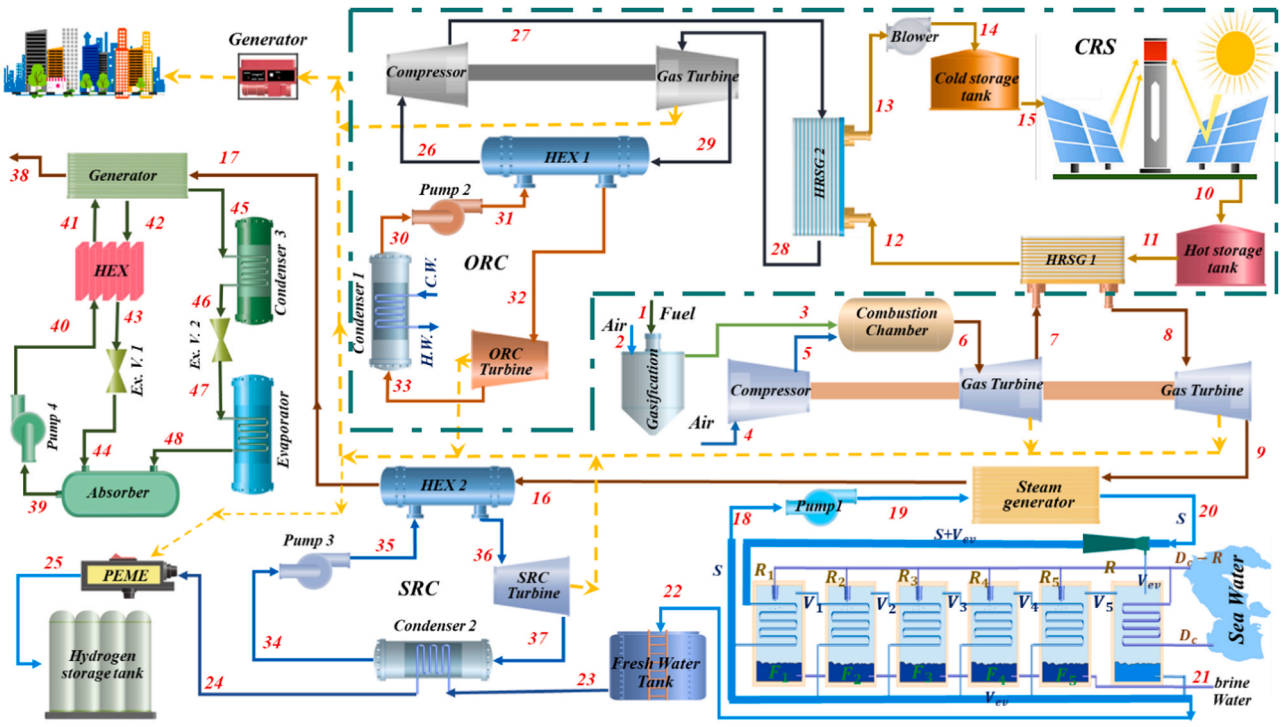


**Fig. 1.** General schematic of the new multi-generation hybrid biomass-solar system.

plants with systems based solely on solar energy by Oyekale et al. (2022) also points to their positive environmental and thermodynamic effects. Recognizing the advantages of renewable energy, Yuan et al. (2024) put forth a heating system that integrates both solar energy and biomass resources. The objective of this system is to decrease energy consumption and minimize $CO_2$ emissions specifically during the warm season.

Mousavi Rabeti et al. (2023) introduced a multi-generation system that utilizes solar and waste resources. After conducting an in-depth analysis and optimization, they discovered that municipal solid waste, with a cost-effective lifespan of 4.28 years, is the most economically viable fuel for the system under investigation. Furthermore, the findings indicated that the system achieves energy and exergy efficiencies of 29.25% and 23.59%, respectively, when operating optimally. A multi-generation system supported by waste solar energy for ammonia production, electricity and heating supply was investigated by Acikalin and Dincer (2023). In this study, a $CO_2$ absorption system was deployed to reduce environmental pollution. Bozgeyik et al. (2023) studied a solar, geothermal and biomass based system for electricity, hydrogen, heating, cooling and fresh water production. Their investigated system with the production of 6.16 kg/s of fresh water had an overall system energy and exergy efficiency of 65.55% and 27.09%.

Based on literature review, thermodynamic and economic analyzes of multi-generation systems with hybrid biomass-solar energy sources is a method for sustainable electricity management. In addition, such combined systems reduce environmental pollution (Bozgeyik et al., 2023). In recent research, a groundbreaking multi-generational system has been developed to effectively mitigate environmental pollution by efficiently managing energy resources based on the specific electricity requirements of a given region. To assess the system's efficiency, a thorough analysis has been conducted, dividing day and night into three distinct periods: on-peak, mid-peak, and off-peak. This approach not only enables significant reduction in the consumption of biomass resources, but also effectively minimizes the release of harmful environmental pollutants. Furthermore, the on-peak period of the analyzed system involved a multi-objective optimization process divided into two categories of objectives. The first category focused on optimizing exergy efficiency, hydrogen production, and fresh water generation while considering the total cost rate of system. The second category, considering the importance of environmental pollutants, sought to simultaneously minimize the total cost rate and $CO_2$ emissions, while maximizing exergy efficiency and fresh water production. Finally, the main contributions of this study are summarized as follows:

- Developing an innovative multi-generation system with hybrid biomass-solar energy that can produce electricity, fresh water, hydrogen, heat and cold air.
- Using solar energy as a heat source of open and closed Brayton cycle in order to increase energy and produce more power.
- Employing the waste heat from subsystems to produce power, heating, cooling, hydrogen and fresh water.
- Comprehensive analysis of the proposed system based on load management using biomass-solar hybrid energy, biomass and solar energy alone.
- Enhancing the efficiency and performance of the system through the hybridization of biomass and solar energy.
- Optimization of the studied system in the on-peak period in three categories by limiting the total cost rate, $CO_2$ emission, and both the total cost rate and $CO_2$ emissions simultaneously.

This paper is organized as follows: after the literature review in the first part, the second section describes the system generally. Then, the next section provides system modeling in more detail in seven subsections. The simulation results are discussed in Section 4. In addition, the system's optimal settings are determined in Section 5. Finally, the last section summarizes the main findings of the paper.

## 2. System description

The present study utilizes biomass, solar, and hybrid biomass-solar energy sources to supply electricity, fresh water, hydrogen, cooling, and heating to meet the demand in the Zahedan region during off-peak, mid-peak, and on-peak times throughout 24 h of the day. A general schematic of the proposed system with hybrid biomass-solar sources is shown in Fig. 1. This multi-generation system includes an open and

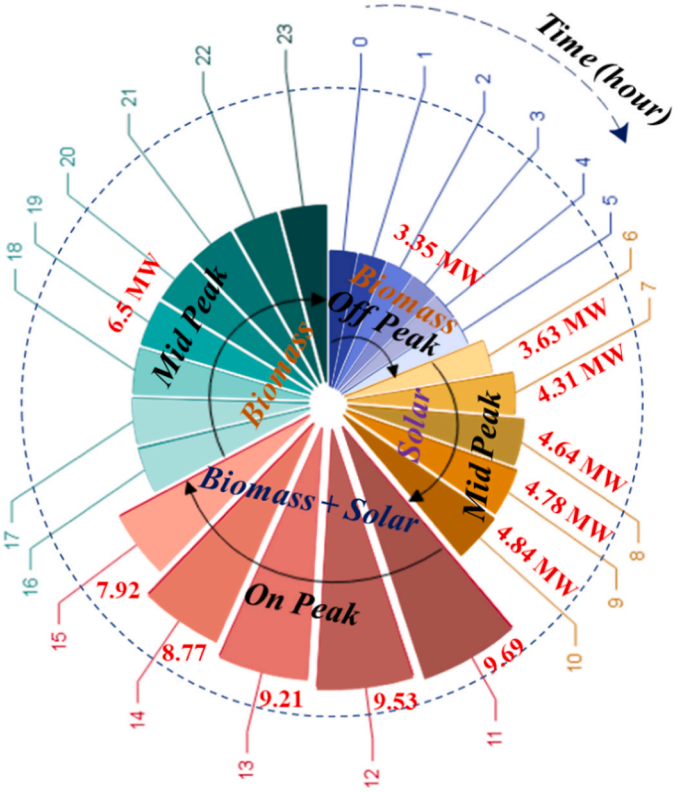


**Fig. 2.** The amount of power required in a typical day (18 August 2019) in Zahedan-Iran.

closed Brayton cycle, solar cycle, SRC, ORC, multi-effect desalination (MED) section, absorption refrigeration cycle, and proton exchange membrane (PEM) electrolyzer. The electricity demand profile at different hours of the day with the type of energy source used is given in Fig. 2.

During the peak period, electricity demand of the area reaches its maximum value; thus, the combined cycle uses a hybrid biomass-solar energy source. As shown in Fig. 1, fuel gasification products (point 3) with compressed air from the compressor (point 5) are added into the combustion chamber. After combustion, the resulting gases enter the gas turbine with a 2% pressure drop and at a temperature of 1370 K (point 6). In this high-pressure gas turbine, exhaust gases are compressed to a pressure of 3.24 bar (point 7) and generate power. These gases are heated by a heat exchanger related to the solar cycle and then are re-entered at high temperatures to generate power in a low-pressure gas turbine (point 8). Further, these gases through the heat exchangers provide the energy needed for the MED section (points 9–16), the SRC (points 16–17), and the absorption refrigeration cycle (points 17–38). The solar cycle also meets the necessary energy for the closed Brayton cycle connected to the ORC (points 12–13). Helium, isobutane, and an ammonia-water mixture are available fluids for closed Brayton cycle, ORC, and absorption refrigeration, respectively. PEM electrolyzer produces hydrogen by consuming electricity and fresh water which is produced from the desalination process (points 24–25). The investigated multi-generation system is supported by biomass energy at off-peak and mid-peak during the night and solar energy at mid-peak during the day.

Below are the assumptions that have been considered during the modeling of the proposed multi-generation system.

- System performance is evaluated in steady state conditions (Xu et al., 2023).
- Heat loss and pressure drop have been ignored along the pipes (Zhang et al., 2022).

**Table 1**
Design parameters of the multi-generation system.

| Parameter | Unit | Value | Reference |
|---|---|---|---|
| Environment temperature | $K$ | 293.15 | (Moharamian et al., 2018) |
| Environment pressure | $kPa$ | 101.325 | (Moharamian et al., 2018) |
| **Solar and biomass subsystems** | | | |
| Cosine effect efficiency ($\eta_{cos}$) | % | 82.67 | (Besarati and Yogi Goswami, 2014) |
| Shading and blocking efficiency ($\eta_{sh\&b}$) | % | 96.98 | (Besarati and Yogi Goswami, 2014) |
| Interception efficiency ($\eta_{int}$) | % | 97.10 | (Besarati and Yogi Goswami, 2014) |
| Atmospheric attenuation efficiency ($\eta_{att}$) | % | 93.83 | (Besarati and Yogi Goswami, 2014) |
| Reflectivity efficiency of heliostats ($\eta_{ref}$) | % | 88.0 | (Besarati and Yogi Goswami, 2014) |
| Direct Normal Irradiance ($DNI$) | $W/m^2$ | 850 | (Zhu et al., 2016) |
| Overall area ($A_{hel}$) of heliostat field | $m^2$ | $9.45 \times 12.84$ | (Zare and Hasanzadeh, 2016) |
| number of heliostat ($N_{hel}$) | - | 624 | (Zare and Hasanzadeh, 2016) |
| Receiver aperture area ($A_{rec}$) | $m^2$ | 68.1 | (Behar et al., 2013) |
| height of the solar tower | $m$ | 130 | (Habibi et al., 2020) |
| Compressor and gas turbine isentropic efficiency | % | 86 | (Anvari et al., 2018) |
| Pump isentropic efficiency | % | 92 | (Anvari et al., 2018) |
| Rankine turbine isentropic efficiency | % | 88 | (Anvari et al., 2018) |
| **Multi-effect Desalination (MED)** | | | |
| MED compression ratio (CR) | - | 2.1 | (Moghimi et al., 2018) |
| Seawater salinity ($X_{fs}$) | $g/kg$ | 36 | (Moghimi et al., 2018) |
| Maximum brine salinity | $g/kg$ | 70 | (Moghimi et al., 2018) |
| Top brine temperature | ℃ | 60 | (Moghimi et al., 2018) |
| Last effect temperature | ℃ | 45 | (Moghimi et al., 2018) |
| **PEM electrolyzer** | | | |
| Operating temperature of PEME ($T_{PEME}$) | ℃ | 80 | (Karunadasa et al., 2012) |
| Activation energy for anode ($E_{act,a}$) | $kJ/mol$ | 76 | (Dai et al., 2023) |
| Activation energy for cathode ($E_{act,c}$) | $kJ/mol$ | 18 | (Dai et al., 2023) |
| Anode water content ($\lambda_a$) | - | 14 | (Dai et al., 2023) |
| Cathode water content ($\lambda_c$) | - | 10 | (Dai et al., 2023) |
| Membrane thickness of PEME ($D$) | $\mu m$ | 50 | (Mehrenjani et al., 2022b) |
| Pre-exponential factor for anode ($J_a^{ref}$) | $A/m^2$ | $1.7 \times 10^5$ | (Nami et al., 2017) |
| Pre-exponential factor for cathode ($J_c^{ref}$) | $A/m^2$ | $4.6 \times 10^3$ | (Nami et al., 2017) |
| Faraday constant ($F$) | ℃$/mol$ | 96.486 | (Karunadasa et al., 2012) |

- Kinetic and potential effects are neglected in the governing conservation equations (Lashgari et al., 2022).
- The oxygen and nitrogen molar coefficients in air are 21.0% and 79.0%, respectively (Dai et al., 2023).

## 3. Modeling

The energy sources of the investigated multi-generation system are based on biomass fuel combustion in the Brayton cycle and supported by a solar heliostat field. Fresh water and hydrogen production is also done by multi-effect desalination and PEM electrolysis. The amount of energy received from biomass and renewable solar sources and the rate of hydrogen and fresh water produced need modeling. Each of these subsystems is separately formulated in the following subsections. Table 1 demonstrates technical characteristics of the proposed system which includes the input parameters of solar and biomass subsystems, MED and PEM electrolyzer.

**Table 2**
Chemical properties of biomass feedstock in the gasifier and the composition percentage of the produced synthesis gas (Zainal et al., 2001).

| Chemical properties | | Produced synthesis gas | |
|---|---|---|---|
| Parameter | Value | Component | Value |
| $CH_{1.44}O_{0.66}$ | – | *Hydrogen*(%) | 21.06 |
| Moisture Content (wt%) | 20 | *Carbon monoxide*(%) | 19.61 |
| C (wt%) | 50 | *Methane*(%) | 0.64 |
| H (wt%) | 6 | *Carbon dioxide*(%) | 12.01 |
| O (wt%) | 44 | *Nitrogen*(%) | 46.68 |

### 3.1. Gasification and combustion model of biomass

In the combustion section, biomass is first converted into gas by the gasification process and is used as a continuous energy source. The type of biomass used in this model is wood with an empirical formula of $CH_{1.44}O_{0.66}$. In addition, Table 2 shows the gases produced from wood gasification (Zainal et al., 2001).

An expression for the general gasification reaction of biomass can be written as follows (Bet Sarkis and Zare, 2018b; Zainal et al., 2001):

$$CH_aO_bN_c + wH_2O + n(O_2 + 3.76N_2) \rightarrow n_1H_2 + n_2CO + n_3CO_2 + n_4H_2O + n_5CH_4 + n_6N_2 \quad (1)$$

In the gasification equation for biomass fuel, $w$ and $n$ are considered for the amount of moisture and oxygen required, respectively. The moisture content ($w$) for biomass fuel is obtained according to Eq. (2). Moreover, MC is the amount of moisture per mole of wood (Bet Sarkis and Zare, 2018b).

$$w = \frac{M_{biomass}\ \ MC}{18(1 - MC)} \quad (2)$$

$$MC = \frac{mass\ \ of\ \ water}{mass\ \ of\ \ wet\ \ biomass} \times 100 \quad (3)$$

The combustion reaction can be expressed chemically as follows (Cao et al., 2021a):

$$n_1H_2 + n_2CO + n_3CO_2 + n_4H_2O + n_5CH_4 + n_6N_2 + n'(O_2 + 3.76N_2) \rightarrow n_7H_2O + n_8CO_2 + n_9O_2 + (n_6 + 3.76n')N_2 \quad (4)$$

The coefficients in relation to gaseous fuel are assumed based on Zainal et al. (2001), and then all the coefficients in the reaction equation are calculated with the balance for H, C, O, and N.

### 3.2. Heliostats field and receiver

The purpose of adding solar energy is to increase power without increasing the amount of biomass fuel, which reduces $CO_2$ emissions. The solar energy received by the heliostat field is transferred to the air passing through it, so that the hot gas exits at point 11 and enters the HRSG1, raising the temperature of the combustion products.

The total radiative energy of the sun absorbed by the heliostat is calculated from Eq. (5) (Zare and Hasanzadeh, 2016).

$$\dot{Q}_{sun} = DNI \times A_{hel} \times N_{hel} \quad (5)$$

In Eq. (5), $N_{hel}$ is the number of the heliostat in the heliostat field, $A_{hel}$ is the overall area, and $DNI$ is the direct normal irradiance received from the heliostat field.

Part of the heat energy absorbed by the heliostat field is lost through conduction and convection to the environment. Therefore, the amount of energy absorbed by the central receiver can be obtained as follows (Zare and Hasanzadeh, 2016):

$$\dot{Q}_{rec,in} = \eta_{field} \times \dot{Q}_{sun} \quad (6)$$

where $\eta_{field}$ is the solar tower heliostat field efficiency and is defined as (Besarati and Yogi Goswami, 2014):

$$\eta_{field} = \eta_{\cos} \times \eta_{s\&b} \times \eta_{\text{int}} \times \eta_{att} \times \eta_{ref} \quad (7)$$

where $\eta_{\cos}$, $\eta_{s\&b}$, $\eta_{\text{int}}$, $\eta_{att}$, and $\eta_{ref}$ represent the cosine effect efficiency, the shading-blocking efficiency, the interception efficiency, the atmospheric attenuation efficiency, and the reflectivity of the heliostats, respectively.

### 3.3. Multi-effect desalination

The MED-TVC unit desalinates seawater in several stages to produce fresh water. As can be seen in the schematic drawn in Fig. 1, seawater with increasing temperature leads to the condensation of steam exiting (V5) from the last stage (MED condenser). The remaining steam from the condenser ($V_{ev}$) enters the ejector with the hot steam (S) exiting from the HRSG (point 20). This hot steam (S+$V_{ev}$) inside the tube acts as a heat source for the first effect of desalination. A portion of the heated seawater is sprayed as seawater effect (R) on the tubes inside which the hot steam is flowing ($V_i$). By transferring heat from the pipe walls, the steam inside the pipes condenses and leads to the evaporation of a part of the salt water sprayed outside the pipes. The steam formed on the outside of the tubes loses its salt and is transferred to the next stage ($V_i$). After that, the mentioned steam heats up the next part of the fluids and it condenses and turns into fresh water. Again, salt water is sprayed on the outer surface of the pipes and evaporates there, and the same process is repeated. Finally, all the fresh water produced is stored in a tank.

The total seawater flow is divided equally in each stage depending on the number of desalination effects. The compressed vapor temperature ($T_{s+v_{ev}}$) entering the first effect is obtained from Eq. (8). Therefore, with the balance of mass and energy, the amount of steam and salt water produced and the salinity of salt water for the steps are calculated according to the following equations (Chitgar and Emadi, 2021; Moghimi et al., 2018).

$$T_{s+v_{ev}} = T_1 + \frac{T_1 - T_N}{N - 1} \quad (8)$$

$$V_i = \frac{(V_{i-1} \times \lambda_{i-1}) - R_i \times C_P(T_{fs}, X_{fs}) \times (T_i - T_{fs})}{(\lambda_i)} + \frac{F_{i-1}C_P(T_{i-1}, X_{i-1}) \times (T_{i-1} - T_i)}{(\lambda_i)} \quad (9)$$

$$F_i = R_i + F_{i-1} - V_i \quad (10)$$

$$X_i = \frac{F_{i-1} \times X_{i-1} + R_i \times X_{fs}}{F_i} \quad (11)$$

where $S$, $V_{ev}$, $N$, $T_i$, $X_{fs}$, $\lambda_i$, and $T_{fs}$ are motive steam flow rate, entrained vapor flow rate, the number of effects, the temperature of effect ($i$), feed seawater salinity, latent evaporation heat at $T_i$, and feed seawater temperature, respectively.

### 3.4. Model of PEM electrolyzer

After separation, water enters electrolyzer where it is converted to oxygen, and hydrogen using electricity. The reaction of the PEME anode electrode is as follows (Razmi et al., 2022):

$$H_2O \rightarrow 2H^+ + \frac{1}{2}O_2 + 2e^- \quad (12)$$

The reaction of the cathode electrode can also be written as follows (Razmi et al., 2022):

$$2H^+ + 2e^- \rightarrow H_2 \quad (13)$$

Therefore, the general reaction for hydrogen production is as follows (Safari and Dincer, 2018):

**Table 3**
Energy and exergy destruction related relations.

| Component | Energy balance equation | Exergy destruction rate |
|---|---|---|
| Gasifier | $\dot{m}_1h_1 + \dot{m}_2h_2 + \dot{Q}_{gasifier} = \dot{m}_3h_3$ | $\dot{E}x_{d,gasifier} = \dot{E}x_1 + \dot{E}x_2 - \dot{E}x_3$ |
| Air compressor | $\dot{m}_4h_4 + \dot{W}_{AC} = \dot{m}_5h_5$ | $\dot{E}x_{d,AC} = \dot{E}x_4 - \dot{E}x_5 + \dot{W}_{AC}$ |
| Combustion chamber | $\dot{m}_3h_3 + \dot{m}_5h_5 + \dot{Q}_{CC} = \dot{m}_6h_6$ | $\dot{E}x_{d,CC} = \dot{E}x_3 + \dot{E}x_5 - \dot{E}x_6$ |
| High pressure gas turbine | $\dot{m}_6h_6 = \dot{m}_7h_7 + \dot{W}_{HP\_GT}$ | $\dot{E}x_{d,HP\_GT} = \dot{E}x_6 - \dot{E}x_7 - \dot{W}_{HP\_GT}$ |
| Low pressure gas turbine | $\dot{m}_8h_8 = \dot{m}_9h_9 + \dot{W}_{LP\_GT}$ | $\dot{E}x_{d,LP\_GT} = \dot{E}x_8 - \dot{E}x_9 - \dot{W}_{LP\_GT}$ |
| HRSG 1 | $\dot{m}_7h_7 + \dot{m}_{11}h_{11} = \dot{m}_8h_8 + \dot{m}_{12}h_{12}$ | $\dot{E}x_{d,HRSG1} = \dot{E}x_7 + \dot{E}x_{11} - \dot{E}x_8 - \dot{E}x_{12}$ |
| Receiver | $\dot{m}_{15}h_{15} + \dot{Q}_{rec} = \dot{m}_{10}h_{10}$ | $\dot{E}x_{d,receiver} = \dot{E}x_{15} - \dot{E}x_{10} + \dot{Q}_{rec,in}\left(1-\frac{T_0}{T_{hel}}\right) - \dot{Q}_{rec,loss}\left(1-\frac{T_0}{T_{rec}}\right)$ |
| Heliostat field | $\dot{Q}_{rec,in} = \eta_{field} \times DNI \times A_{hel} \times N_{hel}$ | $\dot{E}x_{d,hel} = \dot{Q}_{sun}\left(1-\frac{T_0}{T_{sun}}\right) - \dot{Q}_{rec,in}\left(1-\frac{T_0}{T_{hel}}\right)$ |
| HRSG 2 | $\dot{m}_{12}h_{12} + \dot{m}_{27}h_{27} = \dot{m}_{13}h_{13} + \dot{m}_{28}h_{28}$ | $\dot{E}x_{d,HRSG2} = \dot{E}x_{12} + \dot{E}x_{27} - \dot{E}x_{13} - \dot{E}x_{28}$ |
| Air blower | $\dot{W}_{blower} = \dot{m}_{13}h_{13} - \dot{m}_{14}h_{14}$ | $\dot{E}x_{d,blower} = \dot{E}x_{13} - \dot{E}x_{14} + \dot{W}_{blower}$ |
| Steam generator | $\dot{m}_9h_9 + \dot{m}_{19}h_{19} = \dot{m}_{16}h_{16} + \dot{m}_{20}h_{20}$ | $\dot{E}x_{d,Steam\ generator} = \dot{E}x_9 + \dot{E}x_{19} - \dot{E}x_{16} - \dot{E}x_{20}$ |
| Pump 1 | $\dot{m}_{18}h_{18} + \dot{W}_{Pump1} = \dot{m}_{19}h_{19}$ | $\dot{E}x_{d,Pump1} = \dot{E}x_{18} - \dot{E}x_{19} + \dot{W}_{Pump1}$ |
| MED ejector | $\dot{m}_{20}h_{20} + \dot{m}_{V_{ev}}h_{V_{ev}} = \dot{m}_{S+V_{ev}}h_{S+V_{ev}}$ | $\dot{E}x_{d,MED,ejector} = \dot{E}x_{20} + \dot{E}x_{V_{ev}} - \dot{E}x_{S+V_{ev}}$ |
| MED effect *i* | $\dot{m}_{V_{i-1}}h_{V_{i-1}} + \dot{m}_{F_{i-1}}h_{F_{i-1}} + \dot{m}_{R_i}h_{R_i} = \dot{m}_{F_i}h_{F_i} + \dot{m}_{V_i}h_{V_i}$ | $\dot{E}x_{d,MED,eff} = \dot{E}x_{V_{i-1}} + \dot{E}x_{R_i} + \dot{E}x_{F_{i-1}} - \dot{E}x_{F_i} - \dot{E}x_{V_i}$ |
| MED condenser | $\dot{m}_{V_5}h_{V_5} + \dot{m}_{Dc,in}h_{Dc,in} = \dot{m}_{Dc,out}h_{Dc,out} + \dot{m}_{V_{ev}}h_{V_{ev}} + \dot{m}_{V_f}h_{V_f}$ | $\dot{E}x_{d,MED,cond} = \dot{E}x_{V_5} + \dot{E}x_{Dc,in} - \dot{E}x_{Dc,out} - \dot{E}x_{V_{ev}} - \dot{E}x_{V_f}$ |
| Closed Brayton gas turbine | $\dot{m}_{28}h_{28} = \dot{m}_{29}h_{29} + \dot{W}_{GT}$ | $\dot{E}x_{d,GT} = \dot{E}x_{28} - \dot{E}x_{29} - \dot{W}_{GT}$ |
| Closed Brayton compressor | $\dot{m}_{26}h_{26} + \dot{W}_{Comp} = \dot{m}_{27}h_{27}$ | $\dot{E}x_{d,Comp} = \dot{E}x_{26} - \dot{E}x_{27} + \dot{W}_{Comp}$ |
| HEX 1 | $\dot{m}_{29}h_{29} + \dot{m}_{31}h_{31} = \dot{m}_{26}h_{26} + \dot{m}_{32}h_{32}$ | $\dot{E}x_{d,HEX1} = \dot{E}x_{29} + \dot{E}x_{31} - \dot{E}x_{26} - \dot{E}x_{32}$ |
| ORC turbine | $\dot{m}_{32}h_{32} = \dot{m}_{33}h_{33} + \dot{W}_{ORC,Tur}$ | $\dot{E}x_{d,ORC,Tur} = \dot{E}x_{32} - \dot{E}x_{33} - \dot{W}_{ORC,Tur}$ |
| Condenser 1 | $\dot{m}_w(h_{C,W} - h_{H,W}) = \dot{m}_{33}(h_{33} - h_{30})$ | $\dot{E}x_{d,Cond1} = \dot{E}x_{33} + \dot{E}x_{C,W} - \dot{E}x_{30} - \dot{E}_{H,W}$ |
| Pump 2 | $\dot{m}_{30}h_{30} + \dot{W}_{Pump2} = \dot{m}_{31}h_{31}$ | $\dot{E}x_{d,Pump2} = \dot{E}x_{30} - \dot{E}x_{31} + \dot{W}_{Pump2}$ |
| HEX 2 | $\dot{m}_{16}h_{16} + \dot{m}_{35}h_{35} = \dot{m}_{17}h_{17} + \dot{m}_{36}h_{36}$ | $\dot{E}x_{d,HEX2} = \dot{E}x_{16} + \dot{E}x_{35} - \dot{E}x_{17} - \dot{E}x_{36}$ |
| SRC turbine | $\dot{m}_{36}h_{36} = \dot{m}_{37}h_{37} + \dot{W}_{SRC,Tur}$ | $\dot{E}x_{d,SRC,Tur} = \dot{E}x_{36} - \dot{E}x_{37} - \dot{W}_{SRC,Tur}$ |
| Condenser 2 | $\dot{m}_{23}h_{23} + \dot{m}_{37}h_{37} = \dot{m}_{24}h_{24} + \dot{m}_{34}h_{34}$ | $\dot{E}x_{d,Cond2} = \dot{E}x_{23} + \dot{E}x_{37} - \dot{E}x_{24} - \dot{E}x_{34}$ |
| Pump 3 | $\dot{m}_{34}h_{34} + \dot{W}_{Pump3} = \dot{m}_{35}h_{35}$ | $\dot{E}x_{d,Pump3} = \dot{E}x_{34} - \dot{E}x_{35} + \dot{W}_{Pump3}$ |
| PEM electrolyzer | $\dot{m}_{24}h_{24} + \dot{W}_{PEM} = \dot{m}_{25}h_{25} + \dot{m}_{o_2}h_{o_2}$ | $\dot{E}x_{d,PEM} = \dot{E}x_{F,PEM} - \dot{E}x_{P,PEM}$ |
| Generator | $\dot{m}_{17}h_{17} + \dot{m}_{41}h_{41} = \dot{m}_{38}h_{38} + \dot{m}_{42}h_{42} + \dot{m}_{45}h_{45}$ | $\dot{E}x_{d,Generator} = \dot{E}x_{17} + \dot{E}x_{41} - \dot{E}x_{38} - \dot{E}x_{42} - \dot{E}x_{45}$ |
| Pump 4 | $\dot{m}_{39}h_{39} + \dot{W}_{Pump4} = \dot{m}_{40}h_{40}$ | $\dot{E}x_{d,Pump4} = \dot{E}x_{39} - \dot{E}x_{40} + \dot{W}_{Pump4}$ |
| HEX | $\dot{m}_{40}h_{40} + \dot{m}_{42}h_{42} = \dot{m}_{41}h_{41} + \dot{m}_{43}h_{43}$ | $\dot{E}x_{d,HEX} = \dot{E}x_{40} + \dot{E}x_{42} - \dot{E}x_{41} - \dot{E}x_{43}$ |
| Exp. Valve 1 | $\dot{m}_{43}h_{43} = \dot{m}_{44}h_{44}$ | $\dot{E}x_{d,Exp,V1} = \dot{E}x_{43} - \dot{E}x_{44}$ |
| Condenser 3 | $\dot{m}_w(h_{C,W} - h_{H,W}) = \dot{m}_{45}(h_{45} - h_{46})$ | $\dot{E}x_{d,Cond3} = \dot{E}x_{45} + \dot{E}x_{C,W} - \dot{E}x_{46} - \dot{E}x_{H,W}$ |
| Exp. Valve 2 | $\dot{m}_{46}h_{46} = \dot{m}_{47}h_{47}$ | $\dot{E}x_{d,Exp,V2} = \dot{E}x_{46} - \dot{E}x_{47}$ |
| Evaporator | $\dot{m}_{cooling}(h_C - h_H) = \dot{m}_{47}(h_{47} - h_{48})$ | $\dot{E}x_{d,Evap} = \dot{E}x_{47} + \dot{E}x_C - \dot{E}x_{48} - \dot{E}x_H$ |
| Absorber | $\dot{m}_{44}h_{44} + \dot{m}_{48}h_{48} = \dot{m}_{39}h_{39}$ | $\dot{E}x_{d,Absorber} = \dot{E}x_{44} + \dot{E}x_{48} - \dot{E}x_{39}$ |

$$H_2O + \Delta H \rightarrow H_2 + \frac{1}{2}O_2 \tag{14}$$

Here, $\Delta H$ is the total energy required for PEME, which is defined based on $\Delta G$ Gibbs energy and $T\Delta S$ thermal energy as follows (Safari and Dincer, 2018):

$$\Delta H = \Delta G + T\Delta S \tag{15}$$

The molar rate of hydrogen produced by PEME can be defined using current density ($J$) and Faraday constant ($F$) as below (Ni et al., 2008):

$$\dot{N}_{H_2} = \frac{J}{2F} \tag{16}$$

As mentioned earlier, PEME generates hydrogen by consuming electricity. The power required to produce hydrogen in PEME is (Ni et al., 2008):

$$\dot{W}_{PEM} = JV \tag{17}$$

where $V$ is the symbol of cell potential and is defined as follows (Mehrenjani et al., 2022a):

$$V = V_0 + V_{act,a} + V_{act,c} + V_{ohmic} \tag{18}$$

where $V_0$, $V_{act}$ and $V_{ohmic}$ represent reversible potential, over-activation potential, and ohmic potential, respectively. The equations for calculating them are given in Eq. (19) to Eq. (21). In addition, anode and cathode electrodes were indicated by subscripts $a$ and $c$ (Hai et al., 2023).

$$V_0 = 1.229 - 8.5 \times 10^{-4}(T_{PEM} - 298) \tag{19}$$

$$V_{act,i} = \left(\frac{RT}{F}\right)\sinh^{-1}\left(\frac{J}{2J_{0,i}}\right) = \frac{RT}{F}\ln\left(\frac{J}{2J_{0,i}} + \sqrt{\left(\frac{J}{2J_{0,i}}\right)^2 + 1}\right) \tag{20}$$

$$V_{ohmic} = J \times R_{PEM} \tag{21}$$

Here, $R$ is the gas constant, $J_{0,i}$ represents the exchange current density of PEME obtained by Eq. (22), and $R_{PEM}$ is overall ohmic resistance of PEME calculated by Eq. (23) (Hai et al., 2023).

$$J_{0,i} = J_i^{ref}\exp\left(\frac{E_{act,i}}{RT}\right) \tag{22}$$

$$R_{PEM} = \int_0^L \frac{dx}{\sigma_m[\lambda(x)]} \tag{23}$$

Here, $E_{act}$ is the activation energy and $\sigma_m[\lambda(x)]$ represents the local ionic conductivity of PEME membrane and its relation can be presented a: (Ni et al., 2008):

$$\sigma_m[\lambda(x)] = [0.5139\lambda(x) - 326] \times \exp\left[1268\left(\frac{1}{303} - \frac{1}{T}\right)\right] \tag{24}$$

where $\lambda(x)$ is the content of water at x distance, which is defined as follows (Alirahmi et al., 2021):

$$\lambda(x) = \frac{\lambda_a - \lambda_c}{D}x - \lambda_c \tag{25}$$

**Table 4**
Cost functions for each component.

| Component | Reference | Cost function ($Z_k$) |
|---|---|---|
| Gasifier | (Zhang and Sobhani, 2022) | $1600(\dot{m}_{dry\ biomass}\left[\frac{kg}{h}\right])^{0.670}$ |
| Combustion chamber | (Zhang and Sobhani, 2022) | $\left(\frac{46.08\dot{m}_{air}}{0.995-P_{out}/P_{in}}\right)(1+\exp(0.018T_{out}+26.40))$ |
| Gas turbine | (Athari et al., 2017) | $\frac{1536\dot{m}_{gas}}{0.92-\eta_{GT}}\ln\frac{P_i}{P_o}(1+\exp(0.036T_{in}-54.4))$ |
| Compressor | (Zhang and Sobhani, 2022) | $\frac{71.1\dot{m}_{air}}{0.9-\eta_{AC}}\left(\frac{P_{out}}{P_{in}}\right)\ln\frac{P_{out}}{P_{in}}$ |
| heliostat | (Anvari et al., 2018) | $126\times A_{hel}\times N_{hel}$ |
| receiver | (Anvari et al., 2018) | $A_{hel}\times(79\times T_{rec}-42000)$ |
| Blower | (Mehr et al., 2020) | $91562(\dot{W}_{Blower}/455)^{0.67}$ |
| HRSG | (Bet Sarkis and Zare, 2018b) | $4745\left(\frac{\dot{Q}_{HRSG}}{LMTD_{HRSG}}\right)^{0.8}+11820\dot{m}_{steam}+658\dot{m}_{gas}$ |
| Rankine turbine | (Khanmohammadi et al., 2017) | $4750(\dot{W}_{tur})^{0.75}$ |
| Pump | (Baghernejad and Yaghoubi, 2011) | $3540(\dot{W}_{pump})^{0.71}$ |
| Generator | (Cao et al., 2021b) | $130\times(A_{Gen}/0.093)^{0.78}$ |
| Condenser | (Baghernejad and Yaghoubi, 2011) | $1773\times(\dot{m}_{Cond})$ |
| Heat exchanger | (Ghorbani et al., 2020) | $12000(A_{HEX}/100)^{0.6}$ |
| Evaporator | (Cao et al., 2021b) | $1.3\times(190+310A_{Eva})$ |
| Absorber | (Cao et al., 2021b) | $130\times(A_{abs}/0.093)^{0.78}$ |
| Expansion Valve | (Cao et al., 2022b) | $114.5\times\ \dot{m}_{flow}$ |
| Steam generator | (Chitgar and Emadi, 2021) | $8500+409A_{SG}^{0.85}$ |
| MED effects | (Chitgar and Emadi, 2021) | $201.67\times Q\times\Delta T_{LMTD}^{-1}$ |
| MED condenser | (Chitgar and Emadi, 2021) | $430\times0.582\times Q\times\Delta T_{LMTD}^{-1}$ |
| Steam ejector | (Chitgar and Emadi, 2021) | $1000\times16.14\times0.989\times\left(\dot{m}\left(\frac{T_i}{P_i}\right)^{0.05}\right)P_e^{0.75}$ |
| PEM electrolyzer | (Esmaeilion et al., 2022) | $1000\dot{W}_{PEME}$ |

### 3.5. Overall system efficiency

Exergy is the useful work potential in a system at a specified state. Exergy analysis is important for more efficient use of energy. The general equilibrium rate form of exergy is defined as the Eq. (26). The expressions $E\dot{x}_Q$, $E\dot{x}_w$ and $E\dot{x}_d$ represent the exergy of heat transferred, the exergy of work done and the rate of exergy destruction (Vinet and Zhedanov, 2011; Xu et al., 2023).

$$E\dot{x}_Q+\sum_i\dot{m}_i ex_i=\sum_e\dot{m}_e ex_e+E\dot{x}_w+E\dot{x}_d \tag{26}$$

$$E\dot{x}_w=\dot{W}-p_0\frac{dV_{c.v}}{dt} \tag{27}$$

$$E\dot{x}_Q=\dot{Q}_i\times(1-\frac{T_0}{T_i}) \tag{28}$$

The exergy of each state consists of four physical, chemical, kinetic and potential components, which are defined in Eq. (29) to Eq. (32), respectively. Kinetic and potential exergy are neglected due to the insignificance of velocity and height changes (Balali et al., 2023; Khanmohammadi et al., 2023).

$$ex_{ph}=h-h_0-To(s-s_0) \tag{29}$$

$$ex_{ch}=\sum x_k\overline{e}_k^{ch}+\overline{R}T_0\sum x_k\ln x_k \tag{30}$$

$$ex_{kn}=\frac{1}{2}V^2 \tag{31}$$

$$ex_{pt}=gz \tag{32}$$

According to the Eq. (27), the parameters $\dot{W}$ and $\frac{dV_{c.v}}{dt}$ express the time rate of energy transfer by work other than the work flow and the time rate of change of the volume of the control volume itself. The power produced in each section is defined as follows:

$$\dot{W}_{Brayton}=\dot{W}_{\ GT,HP}+\dot{W}_{\ GT,LP}-\dot{W}_{AC} \tag{33}$$

$$\dot{W}_{Rankine}=\dot{W}_{\ SRC,Tur}-\dot{W}_{Pump3}+\dot{W}_{\ ORC,Tur}-\dot{W}_{Pump2} \tag{34}$$

$$\dot{W}_{Others}=\dot{W}_{\ Closed\ Brayton,GT}-\dot{W}_{Closed\ Brayton,AC}-\dot{W}_{Pump1}-\dot{W}_{Pump4}-\dot{W}_{PEME} \tag{35}$$

$$\dot{W}_{\ net}=\dot{W}_{Brayton}+\dot{W}_{Rankine}+\dot{W}_{Others} \tag{36}$$

Chemical exergy is very important in the irreversible chemical reaction where the chemical composition is out of equilibrium. Chemical exergy for the reaction performed in biomass combustion is calculated according to Eq. (37) (Algieri and Morrone, 2022).

$$\overline{ex}_{biomass}^{ch}=\beta\times LHV_{biomass} \tag{37}$$

Here, $\beta$ parameter is defined by the weight fraction of hydrogen ($Z_H$), carbon ($Z_C$), and oxygen ($Z_O$) and obtained according to the following equation (Algieri and Morrone, 2022):

$$\beta=\frac{1.044+0.16\frac{Z_H}{Z_C}-0.34493\frac{Z_O}{Z_C}\left(1+0.0531\frac{Z_H}{Z_C}\right)}{1-0.4142\frac{Z_O}{Z_C}} \tag{38}$$

Exergy efficiency of the system is obtained by dividing the exergy of useful products to total exergy input using Eq. (39):

$$\eta_{Exergy}=\frac{\dot{W}_{\ net}+\dot{E}x_{Heating}+\dot{E}x_{Cooling}+\dot{E}x_{H_2}+\dot{E}x_{MED}}{\dot{E}x_{\ Biomass}+\dot{E}x_{\ Sun}} \tag{39}$$

Table 3 summarizes the energy and exergy balances for each component.

### 3.6. Economic analysis

During the operation of the system, the cost must be considered. Therefore, the system is economically modeled considering the cost of components in different cycles. The cost of each component is calculated according to the maintenance factor ($\phi$) and annual time per hour ($N$) as follows (Nasrabadi and Korpeh, 2023):

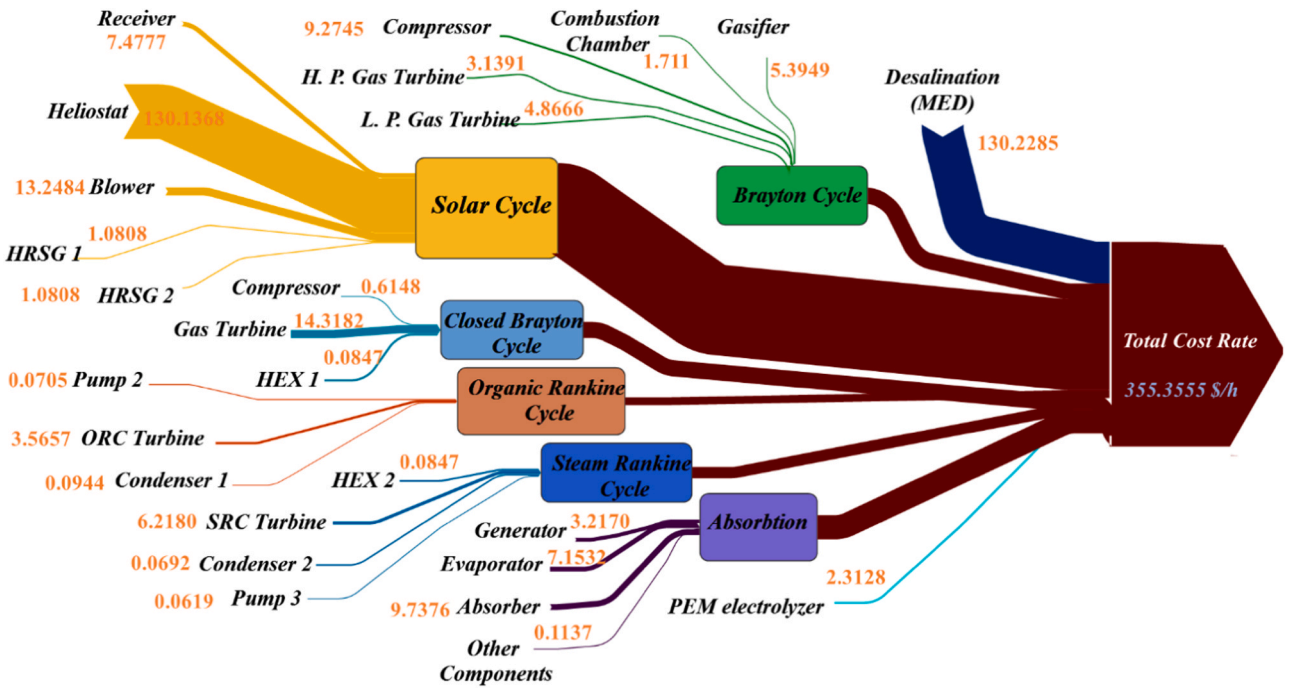


**Fig. 3.** Cost rates of each subsection in the on-peak period.

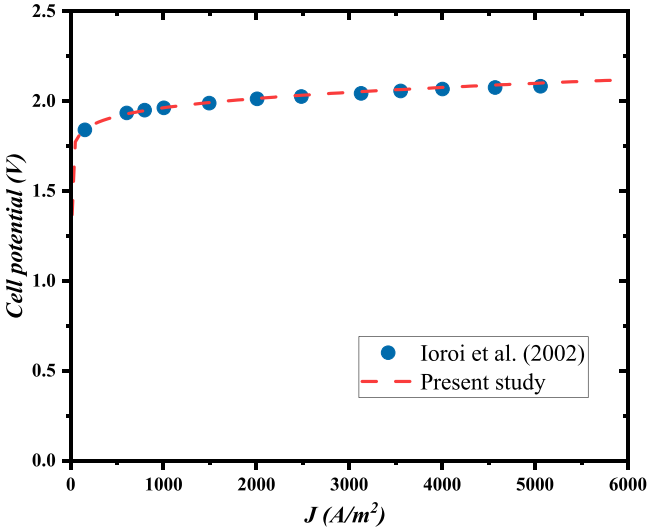


**Fig. 4.** Verification of the simulation models for PEM electrolyzer.

$$\dot{Z}_k = \frac{Z_k \times CRF \times \phi}{N \times 3600}$$

where $Z_k$ represents the cost of purchasing element $k$, which is mentioned in Table 4 for each component. $CRF$ indicating the capital recovery coefficient, which is obtained by Eq. (41) (Seshadri, 1996).

$$CRF = \frac{i(1+i)^n}{(1+i)^n - 1}$$

Here, $i$ represent the interest rate (12%) and $n$ is the service life of the system components (20 years). Based on cost indices, the equipment prices are updated from the initial year to the current year as follows (Mignard, 2014):

$$cost \quad at \quad present \quad year = original \quad cost \times \frac{cost \quad index \quad of \quad the \quad present \quad year}{cost \quad index \quad of \quad the \quad base \quad year}$$

Cost rates of each subsection during the on-peak period with hybrid biomass-solar sources are indicated in Fig. 3. The highest cost rate is related to the solar source with about 36% of the total cost of the system.

### 3.7. Environmental analysis

Findings from the analysis reveal alarming trends of environmental degradation resulting from anthropogenic activities, including industrial pollution, deforestation, habitat destruction, and greenhouse gas emissions. These activities have led to a decline in air and water quality, loss of biodiversity, soil erosion, and alteration of natural habitats (Cuan et al., 2023).

In this regard, in the current study, the effect of biomass-solar hybrid system on $CO_2$ emissions is studied by managing energy resources and the necessary power of the region. Therefore, the amount of $CO_2$ emissions for the system is reported by the following equation (Chen et al., 2023):

$$CO_2 \quad emission = \frac{\dot{m}_{CO_2}}{\dot{W}_{system}} \tag{40}$$

Here, $\dot{m}_{CO_2}$ and $\dot{W}_{system}$ represent the amount of $CO_2$ and the power produced by the system, respectively.

## 4. Result and discussion

### 4.1. Validation

Validation of modeling results in subsystems has been performed. The accuracy of the PEM electrolyzer model was tested considering the cell potential changes by Ioroi et al. (2002). In addition, the fresh water produced in the Multi-effect desalination section was validated by Al-Mutaz and Wazeer (2014). The performed validations demonstrate good agreement as presented in Fig. 4 and Table 5. Furthermore, Table 6 compares the exergy efficiency of the system provided by three existing

**Table 5**
Comparison of the MED study results for the current work with the results presented by Al-Mutaz and Wazeer (2014).

| Plant conditions | Al-Mutaz and Wazeer | Present study |
|---|---|---|
| Operating parameters | | |
| Motive steam pressure (kPa) | 2500 | 2500 |
| Motive steam flow rate (kg/s) | 21.2 | 21.2 |
| Number of effects | 6 | 6 |
| Top brine temperature (℃) | 61.8 | 61.8 |
| Feed seawater temperature (℃) | 40 | 40 |
| Ejector entrainment ratio | 1.36 | 1.36 |
| Minimum brine temperature (℃) | 42.8 | 42.8 |
| Plant performance | | |
| Gain output ratio (GOR) | 8.64 | 8.85 |
| Desalinated water (kg/s) | 183.2 | 187.6 |

**Table 6**
Comparison of exergy efficiency of the investigated system with solar, biomass, and hybrid biomass-solar sources with existing studies.

| Parameter | References | Present study |
|---|---|---|
| Exergy efficiency (Biomass) (%) | 36.03 (Moghimi et al., 2018) | 36.66 |
| Exergy efficiency (Solar) (%) | 23.72 (Okonkwo et al., 2018) | 28.94 |
| Exergy efficiency (hybrid Biomass-Solar) (%) | 24.85 (Anvari et al., 2018) | 29.68 |

studies with the present study. In the article by Moghimi et al. (2018), biomass is used as the only source of energy, and in the article by Okonkwo et al. (2018), solar energy acts as the sole source of the system. Also, in the article of Anvari et al. (2018), the hybrid biomass-solar energy system has been investigated. As can be seen, the results of the present study are better than the existing studies in all three scenarios.

### 4.2. Parametric analysis for the hybrid biomass-solar system

The proposed system is designed to use biomass and solar energy sources. Therefore, the amount of solar radiation is the most sensitive factor that affects the performance of the system. The amount of $CO_2$ emission, total cost rate, exergy efficiency, power, hydrogen, and fresh water produced are the most important outputs of the proposed system. Fig. 5 shows how the system outputs are sensitive to the variability of solar radiation. As can be seen, it is understandable that a rise in solar radiation increases the heat input from the solar part, which leads to more power, hydrogen, and fresh water production and better exergy efficiency. With the increase of solar radiation from 600 to 1000 W/m$^2$, the values of exergy efficiency and total cost rate grow from 24.18% to 32.66% and from 348.71 $/h to 358.25 $/h, respectively. It also causes a 58.4% increase in $CO_2$ emissions and a 2.7% increase in the total cost of the system.

The number of heliostats is the other factor that plays a basic role in the amount of energy received from the sun. The effect of this factor on the performance of the proposed system can be seen in Fig. 6. As seen, an increase in the number of heliostats from 350 to 650, increases electricity generation, exergy efficiency, and total cost rate by 58.9%, 44%, and 29.15%, respectively. In addition, the production of hydrogen and fresh water rises from 3.34 to 5.31 kg/h and from 71.18 to 71.76 kg/s, respectively. Also, the amount of $CO_2$ emission grows from 0.72 to 0.45 tons/MWh.

In the biomass sector, the biomass input flow rate is the most influential factor in the amount of heat released from combustion. By adding to the biomass flow rate in the gasifier, the combustion gases increase. This growth in flow rate produces more power and increases exergy efficiency of the system. The effect of biomass flow rate on system outputs is shown in Fig. 7. As can be seen, by changing the biomass flow rate from 0.5 to 1.5 kg/s, exergy efficiency and net output power grow from 29.12% to 31.82% and from 8.40 to 9.13 MW, respectively. Also, the increase in biomass flow leads to an increase in $CO_2$ emissions from 0.41 to 1.14 tons/MWh and the total cost rate from 354.41 $/h to 359.04 $/h.

Another parameter that affects the system outputs is the compressor pressure ratio. The operation of the investigated multi-generation system with increasing compressor pressure ratio from 5 to 14 is illustrated in Fig. 8. As it can be seen, by increasing the compressor pressure ratio, the output net power increases (from about 6.72–8.28 MW). Exergy efficiency first increases and then decreases. Initially, with the increase in the pressure ratio, the temperature of the compressor outlet air increases, and as a result, the fuel consumption decreases due to reaching the temperature of the gas turbine. But at a pressure ratio greater than 9, the fuel consumption increases and as a result the exergy destruction of the combustion chamber, which has a significant effect on the total exergy destruction, increases and the exergy efficiency decreases. Also, with this action, the amount of $CO_2$ emissions decreases by 17.5% and the total cost rate increases by 4.3%.

A further parameter that affects system efficiency is the inlet temperature of the high-pressure gas turbine (GTIT). As depicted in Fig. 9, increasing GTIT improves all useful outputs of the system. An increase in GTIT makes the combined cycle operate at high temperature and increasing the generation of power, fresh water and hydrogen, and then exergy efficiency. The increase of GTIT from 1000 K to 1500 K increases

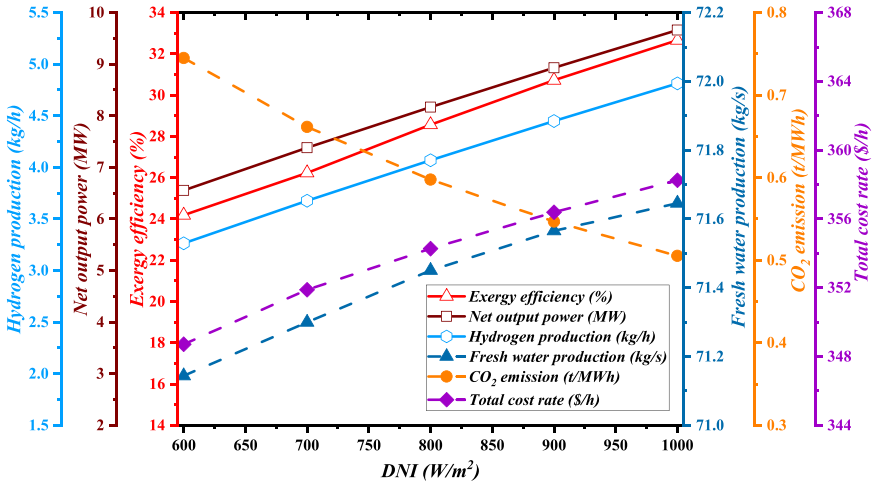


**Fig. 5.** Effect of DNI on the investigated hybrid biomass-solar system.

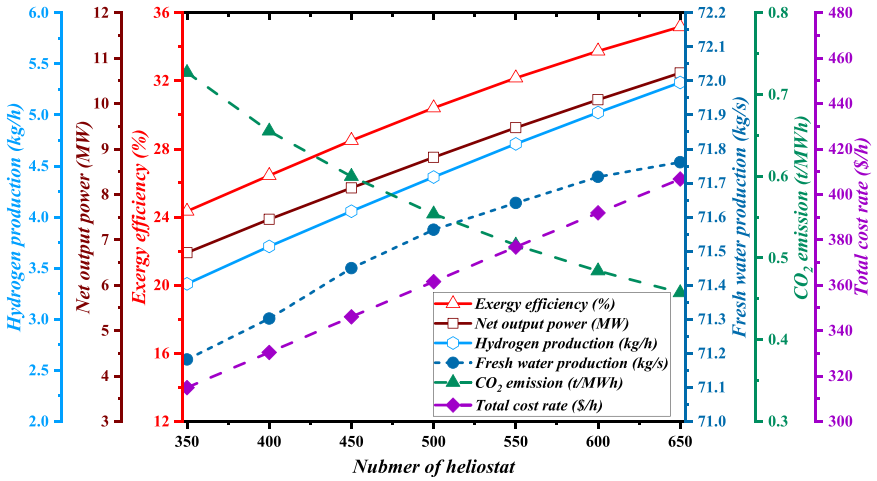


**Fig. 6.** Effect of Number of heliostats on the investigated hybrid biomass-solar system.

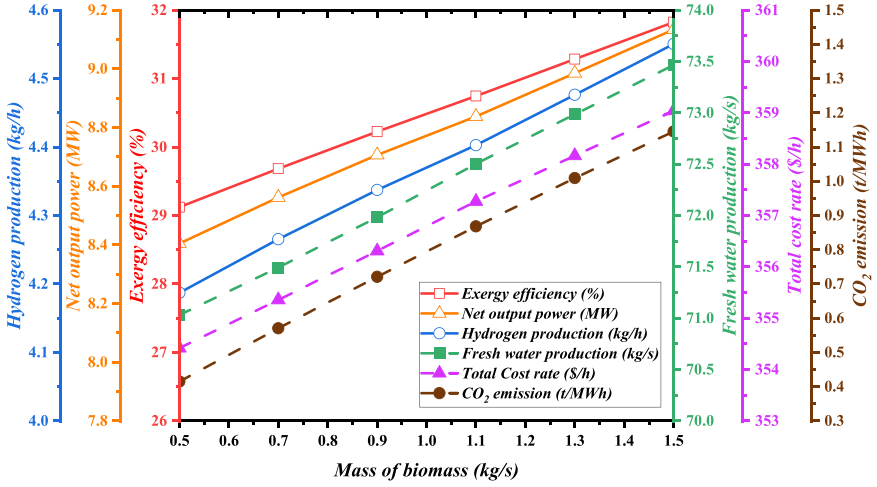


**Fig. 7.** Effect of $\dot{m}_{biomass}$ on the investigated hybrid biomass-solar system.

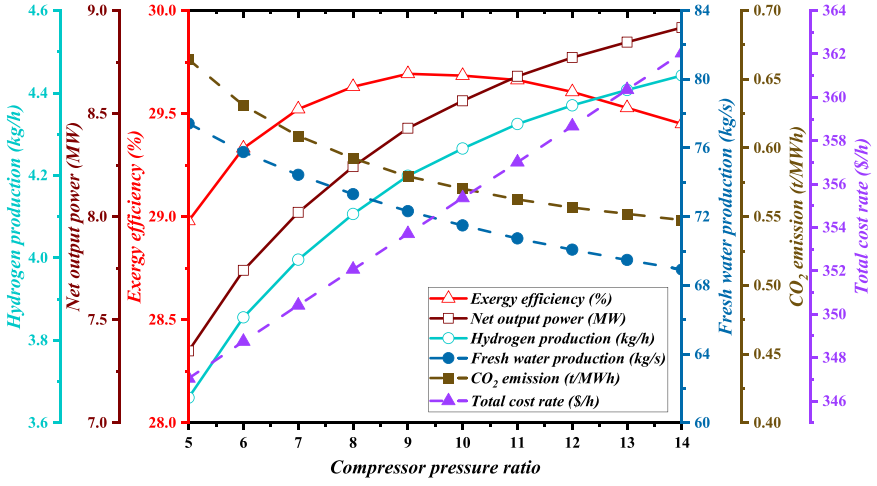


**Fig. 8.** Effect of compressor pressure ratio on the investigated hybrid biomass-solar system.

net output power by 82.9% and leads to a 62.48% improvement in exergy efficiency. The amount of $CO_2$ emission decreases from 0.83 to 0.45 tons/MWh and the total cost rate increases from 351.61 to 358.68 $/h.

The ambient temperature also affects the performance of the investigated hybrid system. The changes of the main outputs of the combined cycle with the increase of the ambient temperature are indicated in Fig. 10. As the ambient temperature increases from 278 to 318 K, the air

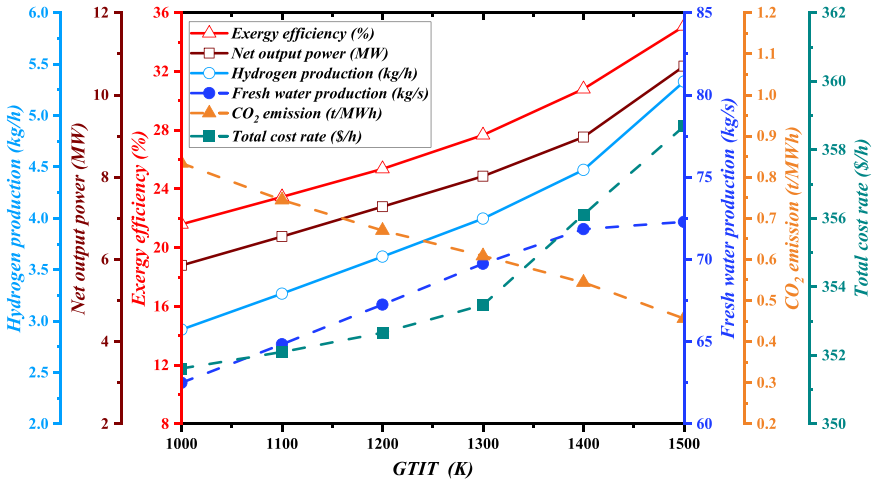


**Fig. 9.** Effect of GTIT on the investigated hybrid biomass-solar system.

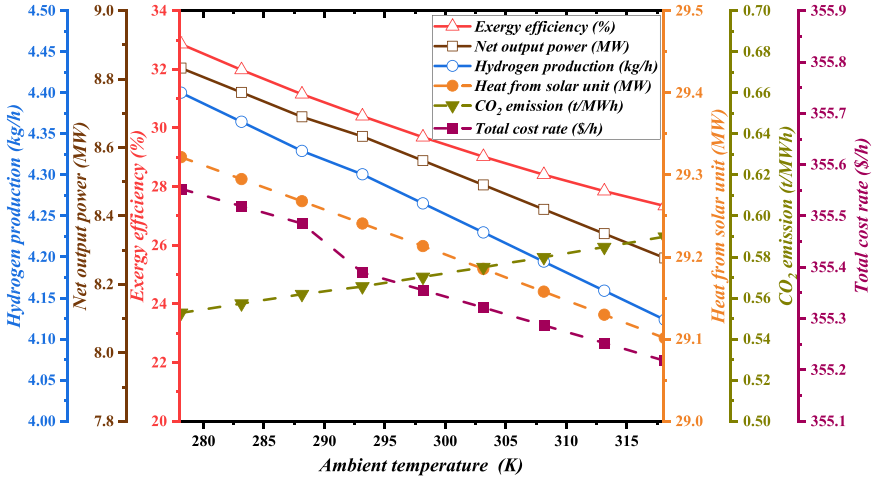


**Fig. 10.** Effect of ambient temperature on the investigated hybrid biomass-solar system.

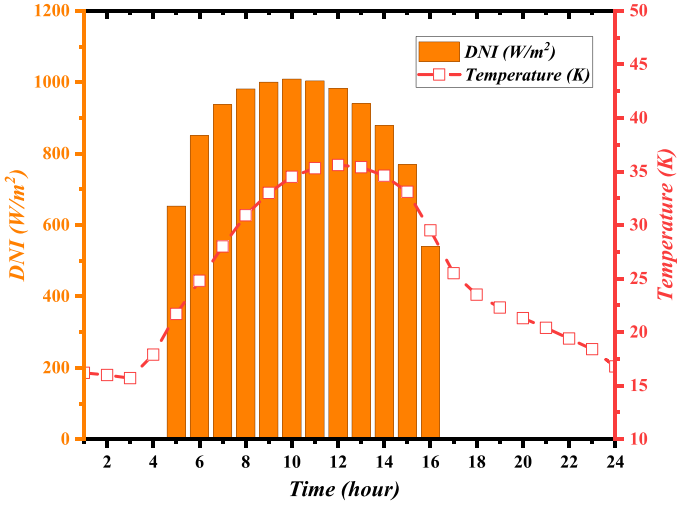


**Fig. 11.** The amount of DNI and temperature during the day of 18 August 2019.

density increases, and the net output power of the system decreases from 8.83214 MW to 8.27704 MW. The production of hydrogen and the total cost of the system are also reduced from 4.4 to 4.12 kg/h and from 355.55 to 355.21 $/h, respectively. Finally, the exergy efficiency decreases from 32.86 to 27.34 and the $CO_2$ emission of the system increases from 0.55 to 0.58 tons/MWh.

### 4.3. Hourly analysis of the system

The present study is evaluated in Zahedan city with the consumption pattern described in Fig. 2 for 24 h a day. On 18 August 2019, the DNI and temperature data for this city were extracted and depicted in Fig. 11. In the current research, according to the pattern of electricity consumption, 24 h of a day are divided into on-peak, mid-peak, and off-peak periods, and biomass, solar and hybrid biomass-solar energies are used as energy sources. The off-peak load time is between 00:00 and 06:00. Due to the unavailability of solar energy, the electricity required during this period is met only by biomass combustion. According to Fig. 2, mid-peak load time is considered between 06:00–11:00 and 16:00–00:00. Between 06:00 and 11:00, solar energy is used and between 16:00 and 00:00, biomass energy is used as an energy source. For on-peak load time between 11:00 and 16:00, the combined cycle is supported by hybrid biomass-solar energy. The use of renewable energy sources based on their availability during different periods leads to biomass storage and less $CO_2$ emissions. So that during mid-peak, the consumption of 6.6 tons of biomass is avoided with the support of solar energy. In addition, duo to the use of hybrid biomass-solar energy during on-peak, the amount of 3.3768 tons of biomass is stored during that period. In Fig. 12, the

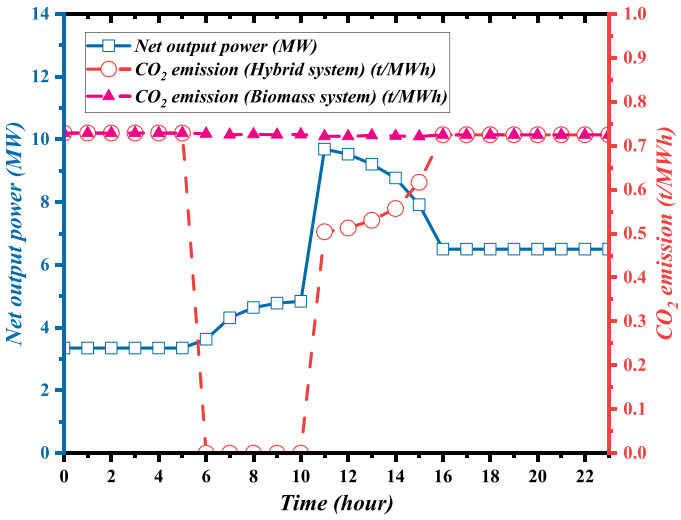


**Fig. 12.** Effect of hybrid biomass-solar system on $CO_2$ emissions during the day.

comparison of $CO_2$ emissions during day and night hours for the system with biomass-solar and biomass sources is reported. The results of modeling for different periods of electricity consumption are reported in Table 7.

## 5. Optimization

The investigated system is a multi-purpose system because of addressing various objectives. Combined cycle optimization is done with the aim of maximizing fresh water, hydrogen production, and exergy efficiency while minimizing total cost rate and $CO_2$ emissions. For this purpose, the multi-objective optimization of the system is performed in two categories of objective functions. In the first category, exergy efficiency, hydrogen and fresh water production are optimized with the constraint of total system cost rate. In the second category, it is optimized by reducing the total cost rate and the amount of $CO_2$ emissions in front of the increase in exergy efficiency and fresh water production.

Number of heliostats ($N_{hel}$), solar cycle mass flow rate ($\dot{m}_{CRS}$), biomass mass flow rate ($\dot{m}_{biomass}$), high-pressure gas turbine inlet temperature ($GTIT$), and compressor pressure ratio ($rp_{comp}$) were selected as the most significant variables, and the range of changes of these variables were presented in Table 8. The genetic algorithm (GA) method that follows the principles of biological evolution has been chosen as the optimization method of the proposed system. The GA strategy to find the optimal solution is iterative and random search. Table 9 presents various optimization considerations that play an important role in influencing the optimization process. These fractions are practically determined as optimal values for various optimization problems and allow faster and more accurate convergence of the process. In each search, the obtained objective functions are compared with their previous values, and the best value of that function is selected as the optimal point, and finally, due to the existence of independent and incomparable points, a set of

**Table 8**
Variation range of decision variables.

| Decision variables | Lower bound | Upper bound | Reason |
|---|---|---|---|
| Number of heliostats ( – ) | 350 | 650 | Economic considerations |
| Solar cycle flow rate ($kg/s$) | 20 | 30 | Environmental limitations |
| Biomass flow rate ($kg/s$) | 0.5 | 1.5 | Environmental limitations |
| Gas turbine inlet temperature ($K$) | 1000 | 1500 | Availability in markets |
| Compressor pressure ratio | 5 | 14 | Availability in markets |

**Table 9**
Some assumptions and considerations of the GA.

| Parameters | Value |
|---|---|
| Mutation fraction | 0.5 |
| Shrink | 0.75 |
| Population size | 100 |
| Cross over fraction | 0.8 |
| Migration fraction | 0.2 |

**Table 7**
The results of the hourly review of the proposed system in Zahedan city on 18 August 2019, depending on the peak time and energy source.

| Time of use period | Source energy | Time (hour) | DNI (W/m$^2$) | Net Output Power (MW) | Hydrogen Production (kg/h) | Fresh water Production (kg/s) | Total Cost Rate ($/h) | Exergy efficiency (%) |
|---|---|---|---|---|---|---|---|---|
| Off-peak | **Biomass** | 0 | 0 | 3.35 | 1.670 | 43.118 | 148.69 | 18.53 |
| | | 1 | 0 | 3.35 | 1.670 | 43.118 | 148.69 | 18.53 |
| | | 2 | 0 | 3.35 | 1.670 | 43.118 | 148.69 | 18.53 |
| | | 3 | 0 | 3.35 | 1.670 | 43.118 | 148.69 | 18.53 |
| | | 4 | 0 | 3.35 | 1.670 | 43.118 | 148.69 | 18.53 |
| | | 5 | 0 | 3.35 | 1.670 | 43.118 | 148.69 | 18.53 |
| Mid-peak | **Solar** | 6 | 850 | 3.63 | 1.813 | 45.422 | 305.32 | 28.94 |
| | | 7 | 937 | 4.31 | 2.149 | 45.490 | 306.98 | 32.61 |
| | | 8 | 981 | 4.64 | 2.312 | 45.521 | 307.75 | 34.23 |
| | | 9 | 1000 | 4.78 | 2.382 | 45.534 | 308.08 | 34.88 |
| | | 10 | 1009 | 4.84 | 2.414 | 45.539 | 308.23 | 35.19 |
| On-peak | **Solar** | 11 | 1004 | 9.69 | 4.828 | 71.646 | 358.31 | 32.97 |
| | + **Biomass** | 12 | 983 | 9.53 | 4.750 | 71.643 | 357.98 | 32.34 |
| | | 13 | 940 | 9.21 | 4.588 | 71.636 | 357.20 | 31.50 |
| | | 14 | 879 | 8.77 | 4.373 | 71.530 | 355.94 | 30.29 |
| | | 15 | 769 | 7.92 | 3.948 | 71.411 | 353.58 | 27.86 |
| Mid-peak | **Biomass** | 16 | 0 | 6.5 | 11.794 | 60.228 | 187.52 | 36.66 |
| | | 17 | 0 | 6.5 | 11.794 | 60.228 | 187.52 | 36.66 |
| | | 18 | 0 | 6.5 | 11.794 | 60.228 | 187.52 | 36.66 |
| | | 19 | 0 | 6.5 | 11.794 | 60.228 | 187.52 | 36.66 |
| | | 20 | 0 | 6.5 | 11.794 | 60.228 | 187.52 | 36.66 |
| | | 21 | 0 | 6.5 | 11.794 | 60.228 | 187.52 | 36.66 |
| | | 22 | 0 | 6.5 | 11.794 | 60.228 | 187.52 | 36.66 |
| | | 23 | 0 | 6.5 | 11.794 | 60.228 | 187.52 | 36.66 |

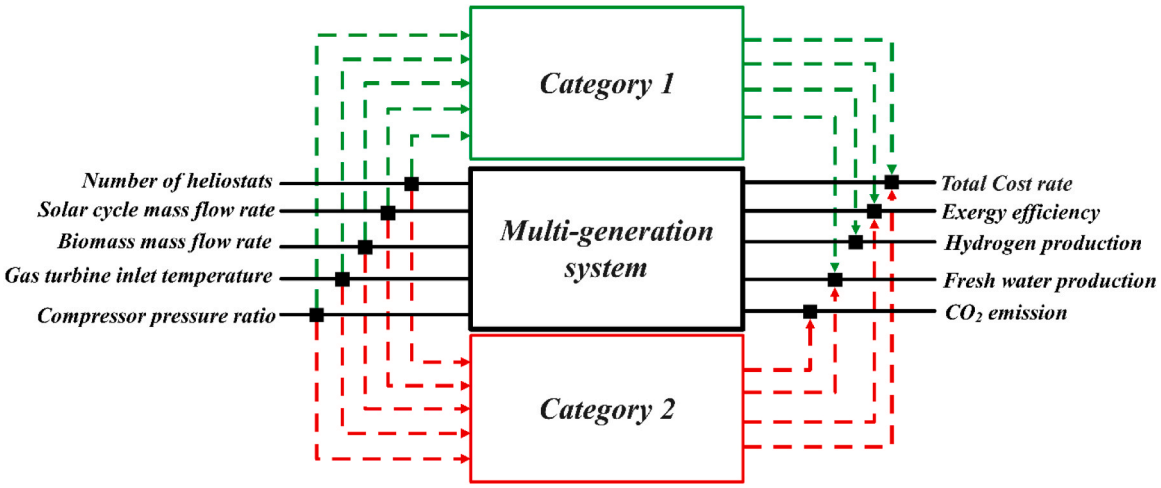


**Fig. 13.** Flowchart for multi-objective optimization of the investigated system.

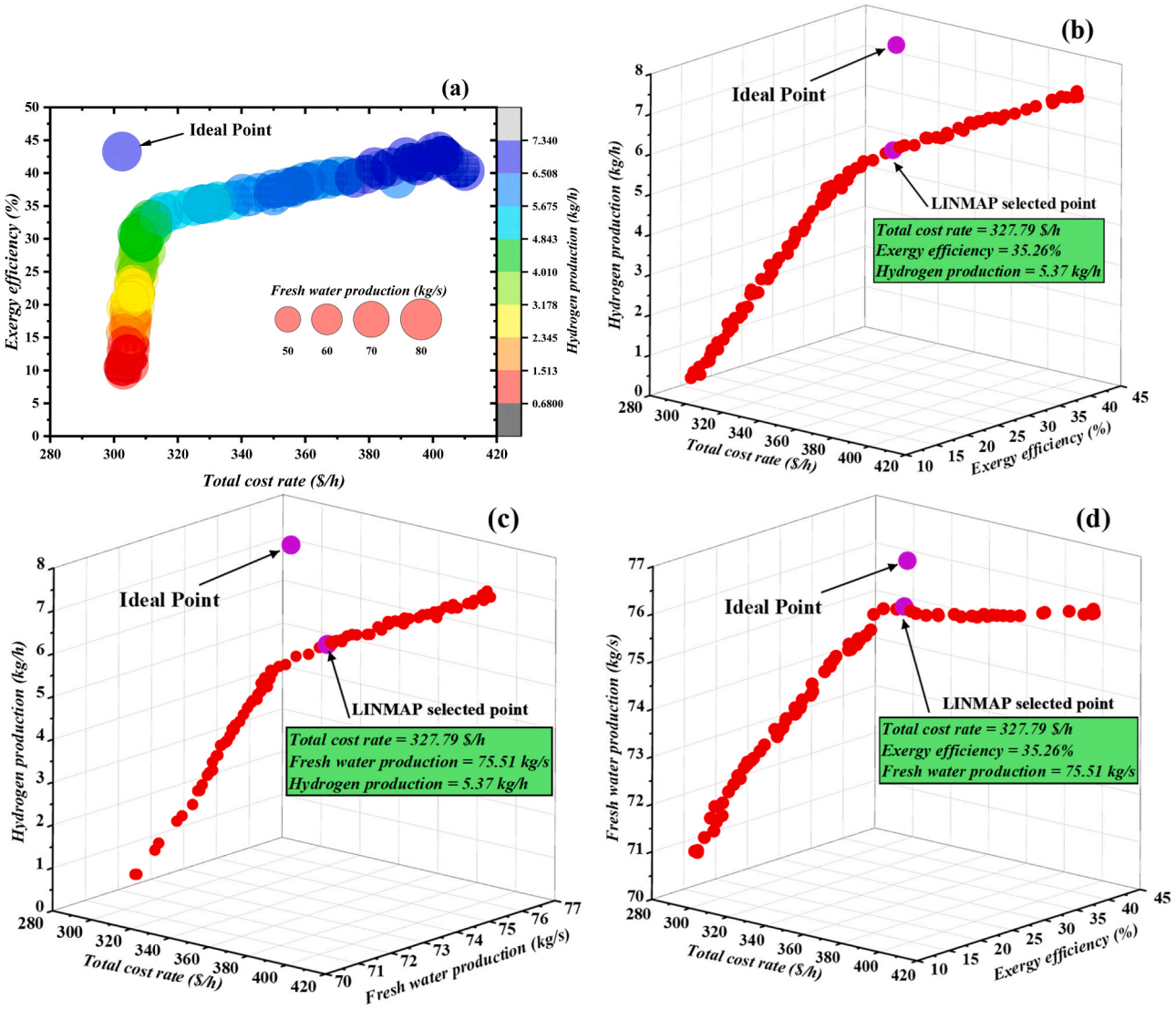


**Fig. 14.** Four-dimensional Pareto frontier diagram considering exergy efficiency, total cost rate, hydrogen and freshwater production as objective functions.

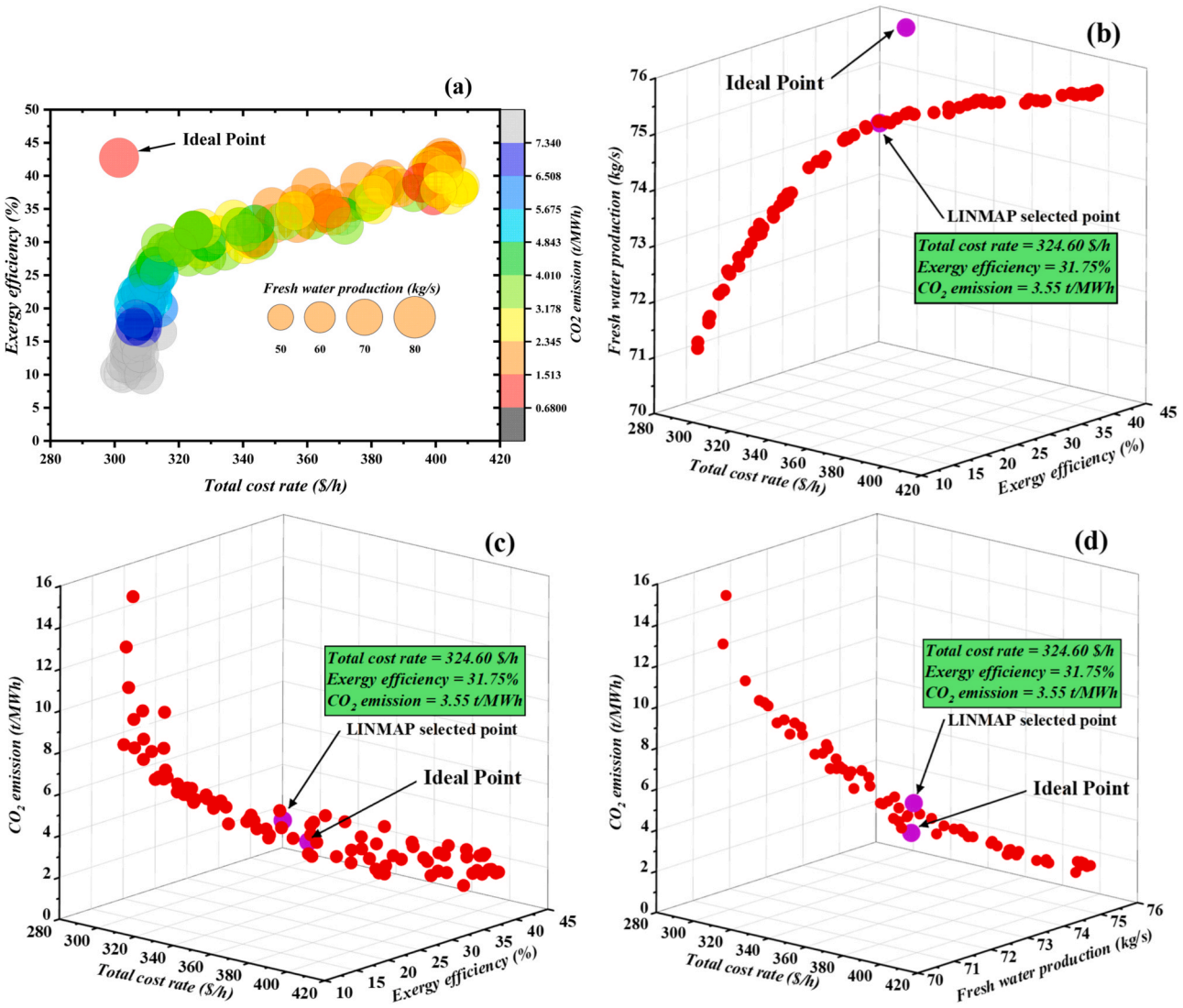


**Fig. 15.** Four-dimensional Pareto frontier diagram considering exergy efficiency, freshwater production, total cost rate, and $CO_2$ emission as objective functions.

**Table 10**
Values of decision variables and objective functions of the system in two categories.

| Category | Objective functions | | | | |
|---|---|---|---|---|---|
| | Exergy efficiency (%) | Hydrogen production ($kg/h$) | Freshwater production ($kg/s$) | Total cost rate ($/h) | $CO_2$ emission (t/$MWh$) |
| 1 | 35.26 | 5.37 | 75.51 | 327.79 | - |
| 2 | 31.75 | - | 74.75 | 324.60 | 3.55 |
| Category | Decision variables | | | | |
| | $N_{heliostat}$ | $\dot{m}_{CRS}$ ($kg/s$) | $\dot{m}_{Biomass}$ ($kg/s$) | GTIT (K) | $rp_{comp}$ |
| 1 | 393.05 | 27.60 | 1.46 | 1490.29 | 5.62 |
| 2 | 385.18 | 26.48 | 1.32 | 1437.52 | 6.17 |

optimal points called the Pareto frontier is obtained instead of an optimal point. To find the optimal point in the Pareto front curve, based on the distance method, LINMAP (Linear Programming Technique for Multidimensional Analysis of Preferences) is utilized. In the LINMAP method, the objective functions are first transformed dimensionless using Eq. (44). The distance of the points in the Pareto front from the hypothetical ideal point (both objective functions are in their optimal state) is calculated by Eq. (46). Since all the points on the Pareto front curve are incomparable to each other, the closest point on the curve to the ideal point is chosen as the preferred optimal point (Mehrenjani et al., 2022b).

$$F_{ij}^{n} = \frac{F_{ij}}{\sqrt[2]{\sum_{i=1}^{m}\left(F_{ij}\right)^{2}}}, j = 1,2,3,4 \tag{41}$$

$$F_{ideal,j}^{n} = \min F_{ij}, j = 1,2,3,4 \tag{42}$$

$$d_{i}^{+} = \sqrt{\sum_{j=1}^{n}\left(F_{ij}{}^{n} - F_{ideal,j}^{n}\right)^{2}} \tag{43}$$

To check the performance and find the optimal solution points from different perspectives, multi-objective optimization was implemented. The hybrid system underwent optimization in two key categories, with primary emphasis on addressing both economic and environmental considerations specifically during peak periods. The first category targeted the minimization of the total cost rate, prioritizing cost efficiency as a primary goal. Meanwhile, the second category aimed to optimize both the $CO_2$ emissions and the total cost rate simultaneously, enabling a dual focus on environmental impact and economic performance. By incorporating these two distinct optimization objectives, the hybrid system sought to strike a balance between financial viability and sustainable practices during peak periods. The flowchart for multi-objective

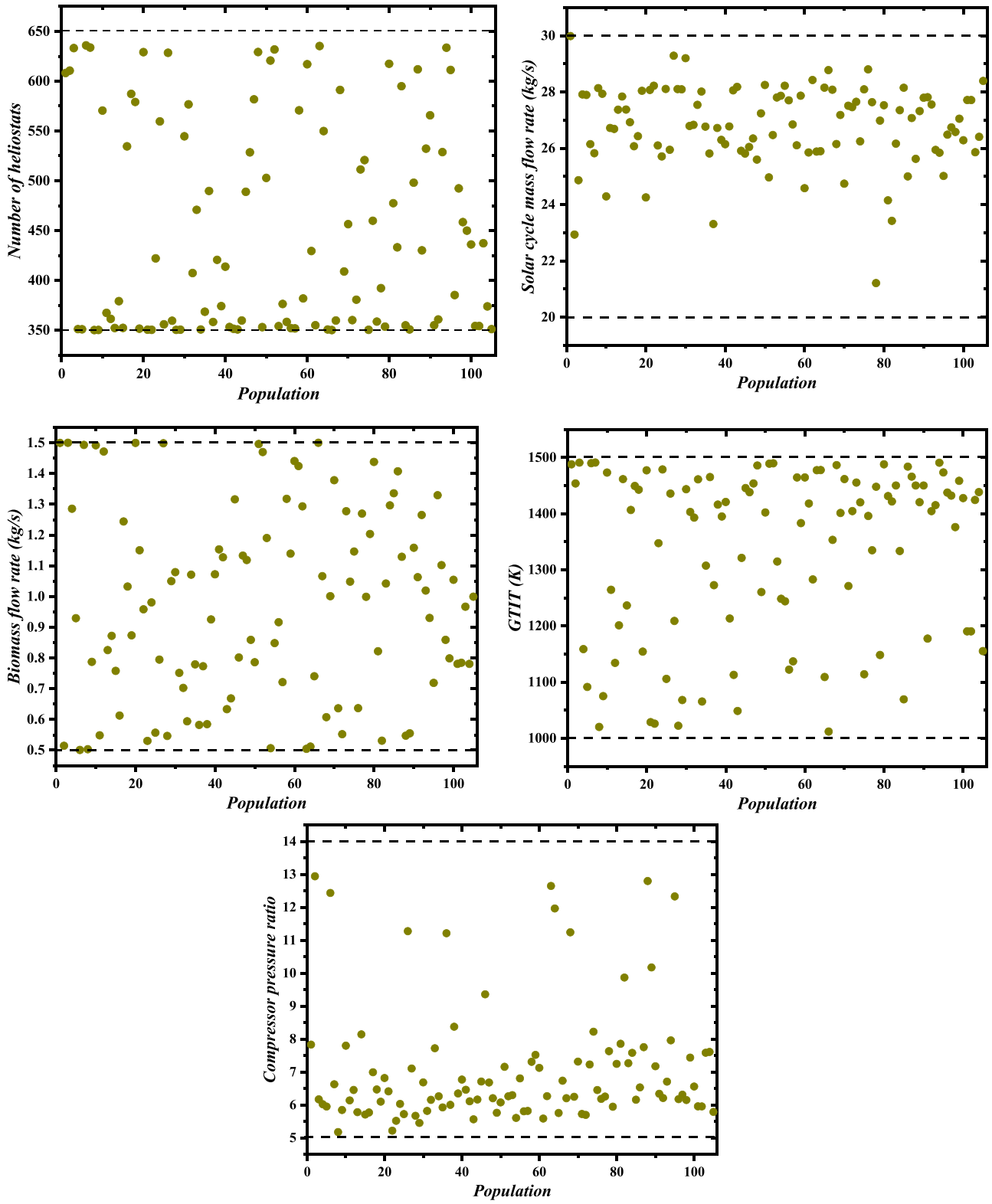


**Fig. 16.** Scatter distribution of decision variables in category 2.

optimization of the investigated system is drawn in Fig. 13. In the first category, optimization is done according to decision variables and objective functions, and its Pareto front diagram is shown in Fig. 14. The ideal point is the point where the total system cost rate is at a minimum and the useful thermodynamic outputs are at their maximum value, which is practically impossible. Therefore, based on the distance method (LINMAP), the closest point of the Pareto front to the ideal point is selected as the most appropriate point. The optimal point selected in the first category has total cost rate, exergy efficiency, hydrogen and fresh water production rate of 327.79 $/h, 35.26%, 5.37 kg/h and 75.51 kg/s, respectively.

For the second category with the objective functions of $CO_2$ emission, total cost rate, exergy efficiency and fresh water production, the Pareto front diagram is depicted in Fig. 15. This category was done due to the

optimal performance of the system with economic and environmental restrictions. At the selected optimal point, the values of $CO_2$ emission, total cost rate, exergy efficiency and fresh water production are 3.55 tons/MWh, 324.60 $/h, 31.75% and 74.75 kg/s, respectively.

The values of decision variables and selected objective functions in three optimization categories for the selected points are reported in Table 10.

Scatter plots provide a visual representation of the relationship between decision variables and objective functions, allowing for quick data insight and analysis. In this regard, Fig. 16 shows the distribution of decision variables. The number of heliostats, gas turbine inlet temperature, and biomass flow rate are critical decision variables that have a potential impact on optimal system performance. According to the diagram, the distribution of these variables is spread over the entire range, which shows their relationship and influence on the objective functions. While the solar cycle mass flow rate and compressor pressure ratio variables are near the upper and lower limits, respectively. Therefore, for optimal system performance, it is appropriate to keep these parameters within the specified range.

## 6. Conclusion

In this study, a multi-generational system was designed with hybrid biomass-solar energy sources capable of cooling, heating, power, hydrogen and freshwater production. The optimal operation of the developed system was investigated for different periods of the day namely off-peak, mid-peak and on-peak based on the electricity consumption pattern in the region. The system is supported at different peaks according to the availability of each energy source at that time. During on-peak, the multi-generation system with hybrid biomass-solar energy support includes open and closed Brayton cycle, solar cycle, steam and organic Rankine cycle, multi-effect desalination section, absorption refrigeration cycle and PEM electrolyzer subsystems. In addition, the optimization of the studied system in the on-peak period was done in two categories by limiting the total cost rate and $CO_2$ emission and the total cost rate simultaneously with the genetic algorithm. Then, using the LINMAP method, the final optimal points were found for the selected objective functions in two categories. Finally, the most important findings of the paper are reviewed as follows:

- The on-peak configuration, which uses hybrid biomass-solar energy, produces more power than the mid-peak and off-peak configurations and leads to an increase in the total cost rate.
- Exergy efficiency of the system during off-peak between 16:00 and 23:00 with biomass source is higher than other configurations.
- Due to the varying intensity of solar radiation throughout the day and its impact on power supply, the effect of solar radiation on the outputs of the hybrid system was evaluated. By changing this parameter between 600 and 1000 $W/m^2$, the net output power generation increased by 47.4%. This led to a 35% improvement in exergy efficiency and a 2.7% growth in the total cost rate. While the amount of $CO_2$ emission drops by 32.4%.
- Using more heliostat mirrors increases the heat received from solar energy. By increasing the number of heliostats from 350 to 650, exergy efficiency increased from 24.34% to 35.17%. But the total cost rate increased sharply from 314.92 $/h to 406.74 $/h. In addition, these changes lead to a decrease in the $CO_2$ emission of the system from 0.72 to 0.45 tons/MWh.
- Biomass energy source is one of the most critical influencing parameters for providing the required outputs of the proposed system. In the hybrid biomass-solar configuration, the effect of biomass fuel on the system function was analyzed. The increase in biomass fuel led to the production of more gases from combustion and ultimately had an upward effect on exergy efficiency, power, total cost rate, and $CO_2$ emission. By changing the biomass flow rate from 0.5 to 1.5 kg/s, the values of exergy efficiency, power, and the total cost rate were improved by 9.28%, 8.68% and 1.3% respectively. Also, the amount of carbon dioxide emission increased from 0.41 to 1.14 tons/MWh and fresh water production from 71.03 to 73.46 kg/s.
- The hybrid system was optimized with a focus on addressing both economic and environmental concerns. At the optimum point, exergy efficiency, fresh water production, total cost rate and $CO_2$ emission were determined to be 31.75%, 74.75 kg/s, 324.60 $/h and 3.55 tons/MWh, respectively.

## Declaration of Competing Interest

The authors declare that they have no known competing financial interests or personal relationships that could have appeared to influence the work reported in this paper.

## References


Acikalin, G., Dincer, I., 2023. A solar based integrated gasification system for municipal plastic wastes to produce multiple useful outputs for environmental protection. Process Saf. Environ. Prot. 178, 776–785. https://doi.org/10.1016/j.psep.2023.08.043.

Algieri, A., Morrone, P., 2022. Thermo-economic investigation of solar-biomass hybrid cogeneration systems based on small-scale transcritical organic Rankine cycles. Appl. Therm. Eng. 210, 118312 https://doi.org/10.1016/j.applthermaleng.2022.118312.

Alirahmi, S.M., Assareh, E., Chitsaz, A., Ghazanfari Holagh, S., Jalilinasrabady, S., 2021. Electrolyzer-fuel cell combination for grid peak load management in a geothermal power plant: Power to hydrogen and hydrogen to power conversion. Int. J. Hydrog. Energy 46, 25650–25665. https://doi.org/10.1016/j.ijhydene.2021.05.082.

Al-Mutaz, I.S., Wazeer, I., 2014. Development of a steady-state mathematical model for MEE-TVC desalination plants. Desalination 351, 9–18. https://doi.org/10.1016/j.desal.2014.07.018.

Altayib, K., Dincer, I., 2022. Design and evaluation of a new solar-biomass based energy system for a small sustainable residential community. J. Clean. Prod. 369, 133275 https://doi.org/10.1016/j.jclepro.2022.133275.

Anvari, S., Khalilarya, S., Zare, V., 2018. Exergoeconomic and environmental analysis of a novel configuration of solar-biomass hybrid power generation system. Energy 165, 776–789. https://doi.org/10.1016/j.energy.2018.10.018.

Athari, H., Soltani, S., Rosen, M.A., Mahmoudi, S.M.S., Morosuk, T., 2017. A comparative exergoeconomic evaluation of biomass post-firing and co-firing combined power plants. Biofuels 8, 1–15. https://doi.org/10.1080/17597269.2016.1194609.

Baghernejad, A., Yaghoubi, M., 2011. Multi-objective exergoeconomic optimization of an Integrated Solar Combined Cycle System using evolutionary algorithms. Int. J. Energy Res. 35, 601–615. https://doi.org/10.1002/er.1715.

Balali, A., Asadabadi, M.J.R., Moghimi, M., 2023. 4E assessment and neural network optimization of a solid oxide fuel cell-based plant with anode and cathode recycling for electricity, freshwater, and hydrogen production. Process Saf. Environ. Prot. 177, 95–117. https://doi.org/10.1016/j.psep.2023.06.066.

Behar, O., Khellaf, A., Mohammedi, K., 2013. A review of studies on central receiver solar thermal power plants. Renew. Sustain. Energy Rev. 23, 12–39. https://doi.org/10.1016/j.rser.2013.02.017.

Besarati, S.M., Yogi Goswami, D., 2014. A computationally efficient method for the design of the heliostat field for solar power tower plant. Renew. Energy 69, 226–232. https://doi.org/10.1016/j.renene.2014.03.043.

Bet Sarkis, R., Zare, V., 2018a. Proposal and analysis of two novel integrated configurations for hybrid solar-biomass power generation systems: thermodynamic and economic evaluation. Energy Convers. Manag. 160, 411–425. https://doi.org/10.1016/j.enconman.2018.01.061.

Bet Sarkis, R., Zare, V., 2018b. Proposal and analysis of two novel integrated configurations for hybrid solar-biomass power generation systems: thermodynamic and economic evaluation. Energy Convers. Manag. 160, 411–425. https://doi.org/10.1016/j.enconman.2018.01.061.

Bozgeyik, A., Altay, L., Hepbasli, A., 2023. Energetic, exergetic, exergoeconomic, environmental and sustainability analyses of a solar, geothermal and biomass based novel multi-generation system for production of power, hydrogen, heating, cooling and fresh water. Process Saf. Environ. Prot. 177, 400–415. https://doi.org/10.1016/j.psep.2023.07.018.

Burulday, M.E., Mert, M.S., Javani, N., 2022. Thermodynamic analysis of a parabolic trough solar power plant integrated with a biomass-based hydrogen production system. Int. J. Hydrog. Energy 47, 19481–19501. https://doi.org/10.1016/j.ijhydene.2022.02.163.

Cao, Y., Dhahad, H.A., Togun, H., Anqi, A.E., Farouk, N., Farhang, B., 2021a. A novel hybrid biomass-solar driven triple combined power cycle integrated with hydrogen production: multi-objective optimization based on power cost and $CO_2$ emission. Energy Convers. Manag. 234, 113910 https://doi.org/10.1016/j.enconman.2021.113910.

Cao, Y., Mihardjo, L.W.W., Dahari, M., Tlili, I., 2021b. Waste heat from a biomass fueled gas turbine for power generation via an ORC or compressor inlet cooling via an absorption refrigeration cycle: a thermoeconomic comparison. Appl. Therm. Eng. 182, 116117 https://doi.org/10.1016/j.applthermaleng.2020.116117.

Cao, Y., Alsharif, S., ATTIA, E.A., Shamseldin, M.A., Ibrahim, B.F., 2022a. A conceptual process design towards $CO_2$ emission reduction by integration of solar-based hydrogen production and injection into biomass-derived solid oxide fuel cell. Process Saf. Environ. Prot. 164, 164–176. https://doi.org/10.1016/j.psep.2022.05.050.

Cao, Y., Dhahad, H.A., Sharma, K., Anqi, A.E., El-Shafay, A.S., Najat Ahmed, A., 2022b. Comprehensive thermodynamic and economic analyses and optimization of a novel poly-generation setup utilizing solar and geothermal sources. Appl. Therm. Eng. 207, 118133 https://doi.org/10.1016/j.applthermaleng.2022.118133.

Chen, F., Zhang, W., Liu, Y., Cai, J., Zhang, J.L., Wang, X.M., Su, Q., 2023. Simulation and 4E analysis of a novel trigeneration process using a gas turbine cycle combined with a geothermal-driven multi-waste heat recovery method. Process Saf. Environ. Prot. 176, 1026–1047. https://doi.org/10.1016/j.psep.2023.06.078.

Chitgar, N., Emadi, M.A., 2021. Development and exergoeconomic evaluation of a SOFC-GT driven multi-generation system to supply residential demands: Electricity, fresh water and hydrogen. Int. J. Hydrog. Energy 46, 17932–17954. https://doi.org/10.1016/j.ijhydene.2021.02.191.

Cuan, Z., Chen, Y., Kumar, M.S., 2023. Design, multi-aspect analyses, and multi-objective optimization of a novel trigeneration system based on geothermal and municipal solid waste energies. Process Saf. Environ. Prot. 177, 581–597. https://doi.org/10.1016/j.psep.2023.06.062.

Dai, J., Abdulwahab, A., Wei, H., Alanazi, A., Alanazi, M., I Alanazi, T., Armghan, A., Wae-hayee, M., 2023. Multi-criteria sensitivity study and optimization of an electricity/cooling/hydrogen production scheme combined with SOFC-based sequential heat recovery: Sustainability and economic analyses. Process Saf. Environ. Prot. 174, 169–187. https://doi.org/10.1016/j.psep.2023.03.083.

Devi, L., Ptasinski, K.J., Janssen, F.J.J.G., 2003. A review of the primary measures for tar elimination in biomass gasification processes. Biomass-.-. Bioenergy 24, 125–140. https://doi.org/10.1016/S0961-9534(02)00102-2.

Esmaeilion, F., Soltani, M., Nathwani, J., Al-Haq, A., 2022. Design, analysis, and optimization of a novel poly-generation system powered by solar and wind energy. Desalination 543, 116119. https://doi.org/10.1016/j.desal.2022.116119.

Ghorbani, S., Khoshgoftar-Manesh, M.H., Nourpour, M., Blanco-Marigorta, A.M., 2020. Exergoeconomic and exergoenvironmental analyses of an integrated SOFC-GT-ORC hybrid system. Energy 206, 507–519. https://doi.org/10.1016/j.energy.2020.118151.

Habibi, H., Zoghi, M., Chitsaz, A., Javaherdeh, K., Ayazpour, M., Bellos, E., 2020. Working fluid selection for regenerative supercritical Brayton cycle combined with bottoming ORC driven by molten salt solar power tower using energy–exergy analysis. Sustain. Energy Technol. Assess. 39, 100699 https://doi.org/10.1016/j.seta.2020.100699.

Hai, T., Mansir, I.B., yakoop, A. khudhair, Mulki, H., Anqi, A.E., Deifalla, A., Chen, Y., 2023. Integration of wind turbine with biomass-fueled SOFC to provide hydrogen-rich fuel: Economic and $CO_2$ emission reduction assessment. Process Saf. Environ. Prot. 170, 946–959. https://doi.org/10.1016/j.psep.2022.12.049.

Ioroi, T., Yasuda, K., Siroma, Z., Fujiwara, N., Miyazaki, Y., 2002. Thin film electrocatalyst layer for unitized regenerative polymer electrolyte fuel cells. J. Power Sources 112, 583–587. https://doi.org/10.1016/S0378-7753(02)00466-4.

Jie Ling, J.L., Go, E.S., Park, Y.K., Lee, S.H., 2022. Recent advances of hybrid solar - Biomass thermo-chemical conversion systems. Chemosphere 290, 133245. https://doi.org/10.1016/j.chemosphere.2021.133245.

Karunadasa, H.I., Montalvo, E., Sun, Y., Majda, M., Long, J.R., Chang, C.J., 2012. A molecular MoS2 edge site mimic for catalytic hydrogen generation. Science 335, 698–702. https://doi.org/10.1126/science.1215868.

Khanmohammadi, S., Heidarnejad, P., Javani, N., Ganjehsarabi, H., 2017. Exergoeconomic analysis and multi objective optimization of a solar based integrated energy system for hydrogen production. Int. J. Hydrog. Energy 42, 21443–21453. https://doi.org/10.1016/j.ijhydene.2017.02.105.

Khanmohammadi, S., Razi, S., Delpisheh, M., Panchal, H., 2023. Thermodynamic modeling and multi-objective optimization of a solar-driven multi-generation system producing power and water. Desalination 545, 116158. https://doi.org/10.1016/j.desal.2022.116158.

Kumar, P., Pal, N., Sharma, H., 2022. Optimization and techno-economic analysis of a solar photo-voltaic/biomass/diesel/battery hybrid off-grid power generation system for rural remote electrification in eastern India. Energy 247, 123560. https://doi.org/10.1016/j.energy.2022.123560.

Lashgari, F., Babaei, S.M., Pedram, M.Z., Arabkoohsar, A., 2022. Comprehensive analysis of a novel integration of a biomass-driven combined heat and power plant with a compressed air energy storage (CAES). Energy Convers. Manag. 255, 115333 https://doi.org/10.1016/j.enconman.2022.115333.

Mehr, A.S., Moharramian, A., Hossainpour, S., Pavlov, D.A., 2020. Effect of blending hydrogen to biogas fuel driven from anaerobic digestion of wastewater on the performance of a solid oxide fuel cell system. Energy 202, 117668. https://doi.org/10.1016/j.energy.2020.117668.

Mehrenjani, J.R., Gharehghani, A., Nasrabadi, A.M., Moghimi, M., 2022a. Design, modeling and optimization of a renewable-based system for power generation and hydrogen production. Int. J. Hydrog. Energy 47, 14225–14242. https://doi.org/10.1016/j.ijhydene.2022.02.148.

Mehrenjani, J.R., Gharehghani, A., Sangesaraki, A.G., 2022b. Machine learning optimization of a novel geothermal driven system with LNG heat sink for hydrogen production and liquefaction. Energy Convers. Manag. 254, 115266 https://doi.org/10.1016/j.enconman.2022.115266.

Mignard, D., 2014. Correlating the chemical engineering plant cost index with macro-economic indicators. Chem. Eng. Res. Des. 92, 285–294. https://doi.org/10.1016/j.cherd.2013.07.022.

Moghimi, M., Emadi, M., Mirzazade Akbarpoor, A., Mollaei, M., 2018. Energy and exergy investigation of a combined cooling, heating, power generation, and seawater desalination system. Appl. Therm. Eng. 140, 814–827. https://doi.org/10.1016/j.applthermaleng.2018.05.092.

Moharamian, A., Soltani, S., Rosen, M.A., Mahmoudi, S.M.S., 2018. Exergoeconomic and thermodynamic analyses of an externally fired combined cycle with hydrogen production and injection to the combustion chamber. Int. J. Hydrog. Energy 43, 781–792. https://doi.org/10.1016/j.ijhydene.2017.11.136.

Mousavi Rabeti, S.A., Khoshgoftar Manesh, M.H., Amidpour, M., 2023. An innovative optimal 4E solar-biomass waste polygeneration system for power, methanol, and freshwater production. J. Clean. Prod. 412, 137267 https://doi.org/10.1016/j.jclepro.2023.137267.

Nami, H., Akrami, E., Ranjbar, F., 2017. Hydrogen production using the waste heat of Benchmark pressurized Molten carbonate fuel cell system via combination of organic Rankine cycle and proton exchange membrane (PEM) electrolysis. Appl. Therm. Eng. 114, 631–638. https://doi.org/10.1016/j.applthermaleng.2016.12.018.

Nami, H., Anvari-Moghaddam, A., Nemati, A., 2021. Modeling and analysis of a solar boosted biomass-driven combined cooling, heating and power plant for domestic applications. Sustain. Energy Technol. Assess. 47, 101326 https://doi.org/10.1016/j.seta.2021.101326.

Nasrabadi, A.M., Korpeh, M., 2023. Techno-economic analysis and optimization of a proposed solar-wind-driven multigeneration system; case study of Iran. Int. J. Hydrog. Energy. https://doi.org/10.1016/j.ijhydene.2022.12.283.

Ni, M., Leung, M.K.H., Leung, D.Y.C., 2008. Energy and exergy analysis of hydrogen production by a proton exchange membrane (PEM) electrolyzer plant. Energy Convers. Manag. 49, 2748–2756. https://doi.org/10.1016/j.enconman.2008.03.018.

Okonkwo, E.C., Okwose, C.F., Abid, M., Ratlamwala, T.A.H., 2018. Second-law analysis and exergoeconomics optimization of a solar tower–driven combined-cycle power plant using supercritical $CO_2$. J. Energy Eng. 144, 4018021. https://doi.org/10.1061/(asce)ey.1943-7897.0000534.

Oner, O., Dincer, I., 2022. A unique solar and biomass-based system for integrated production of electricity, heat, freshwater, hydrogen and ethanol. Energy Convers. Manag. 269, 116115 https://doi.org/10.1016/j.enconman.2022.116115.

Oyekale, J., Petrollese, M., Cocco, D., Cau, G., 2022. Annualized exergoenvironmental comparison of solar-only and hybrid solar-biomass heat interactions with an organic Rankine cycle power plant. Energy Convers. Manag. X 15, 100229. https://doi.org/10.1016/j.ecmx.2022.100229.

Pantaleo, A.M., Camporeale, S.M., Sorrentino, A., Miliozzi, A., Shah, N., Markides, C.N., 2020. Hybrid solar-biomass combined Brayton/organic Rankine-cycle plants integrated with thermal storage: Techno-economic feasibility in selected Mediterranean areas. Renew. Energy 147, 2913–2931. https://doi.org/10.1016/j.renene.2018.08.022.

Razmi, A.R., Alirahmi, S.M., Nabat, M.H., Assareh, E., Shahbakhti, M., 2022. A green hydrogen energy storage concept based on parabolic trough collector and proton exchange membrane electrolyzer/fuel cell: Thermodynamic and exergoeconomic analyses with multi-objective optimization. Int. J. Hydrog. Energy 47, 26468–26489. https://doi.org/10.1016/j.ijhydene.2022.03.021.

Safari, F., Dincer, I., 2018. Assessment and optimization of an integrated wind power system for hydrogen and methane production. Energy Convers. Manag. 177, 693–703. https://doi.org/10.1016/j.enconman.2018.09.071.

Seshadri, K., 1996. Thermal design and optimization. Energy. John Wiley & Sons. https://doi.org/10.1016/s0360-5442(96)90000-6.

Suresh, N.S., Thirumalai, N.C., Dasappa, S., 2019. Modeling and analysis of solar thermal and biomass hybrid power plants. Appl. Therm. Eng. 160, 114121 https://doi.org/10.1016/j.applthermaleng.2019.114121.

Vinet, L., Zhedanov, A., 2011. A "missing" family of classical orthogonal polynomials. Journal of Physics A: Mathematical and Theoretical. McGraw-hill New York. https://doi.org/10.1088/1751-8113/44/8/085201.

Xu, J., Su, Z., Meng, J., Yao, Y., Vafadaran, M.S., Kiani Salavat, A., 2023. A thermodynamic, exergoeconomic, and exergoenvironmental investigation and optimization on a novel geothermal trigeneration system to sustain a sport arena. Process Saf. Environ. Prot. 177, 278–298. https://doi.org/10.1016/j.psep.2023.07.017.

Yuan, P., Duanmu, L., Wang, Z., Gao, S., Zheng, H., 2024. Thermal performance of solar-biomass energy heating system coupled with thermal storage floor and radiators in northeast China. Appl. Therm. Eng. 236, 121458 https://doi.org/10.1016/j.applthermaleng.2023.121458.

Zainal, Z.A., Ali, R., Lean, C.H., Seetharamu, K.N., 2001. Prediction of performance of a downdraft gasifier using equilibrium modeling for different biomass materials. Energy Convers. Manag. 42, 1499–1515. https://doi.org/10.1016/S0196-8904(00)00078-9.

Zare, V., Hasanzadeh, M., 2016. Energy and exergy analysis of a closed Brayton cycle-based combined cycle for solar power tower plants. Energy Convers. Manag. 128, 227–237. https://doi.org/10.1016/j.enconman.2016.09.080.

Zhang, F. yang, Feng, Y. qiang, He, Z. xia, Xu, J. wei, Zhang, Q., Xu, K. jing, 2022. Thermo-economic optimization of biomass-fired organic Rankine cycles combined heat and power system coupled $CO_2$ capture with a rated power of 30 kW. Energy 254, 124433. https://doi.org/10.1016/j.energy.2022.124433.

Zhang, L., Sobhani, B., 2022. Comprehensive economic analysis and multi-objective optimization of an integrated power and freshwater generation cycle based on flash-binary geothermal and gas turbine cycles. J. Clean. Prod. 364, 61–79. https://doi.org/10.1016/j.jclepro.2022.132644.

Zhu, Y., Zhai, R., Peng, H., Yang, Y., 2016. Exergy destruction analysis of solar tower aided coal-fired power generation system using exergy and advanced exergetic methods. Appl. Therm. Eng. 108, 339–346. https://doi.org/10.1016/j.applthermaleng.2016.07.116.